Available online at www.sciencedirect.com

ScienceDirect

Geochimica et Cosmochimica Acta 300 (2021) 279–295

Geochimica et Cosmochimica Acta

www.elsevier.com/locate/gca

Micro-distribution of oxygen isotopes in unequilibrated enstatite chondrites

Michael K. Weisberg [a,b,c], Noriko T. Kita [d], Kohei Fukuda [d], Guillaume Siron [d], Denton S. Ebel [b,c]

[a] Dept. Physical Sci., Kingsborough College CUNY, Brooklyn, NY 11235, United States
[b] Dept. Earth and Environmental Sci., CUNY Graduate Center, New York, NY 10016, United States
[c] Dept. Earth and Planetary Sci., American Museum of Natural History, New York, NY 10024, United States
[d] WiscSIMS, Dept. of Geoscience, University of Wisconsin-Madison, Madison, WI 53706, United States

Received 23 September 2020; accepted in revised form 16 February 2021; Available online 25 February 2021

Abstract

We report petrology and high precision, *in situ* oxygen isotope analyses of silicates in chondrules, fragments, metal-rich nodules and refractory inclusions from the ALH 81189 (EH3), ALH 85159 (paired with ALH 81189) and from the MAC 88136 (EL3) chondrite. This is the first report of oxygen isotope ratios for individual objects in an EL3 and for the silicates associated with the metal-rich nodules that are characteristic of unequilibrated enstatite (E3) chondrites. The oxygen isotopic data from the chondrules and other objects form a trend, on a 3-isotope plot, that coincides with the slope ~1 primitive chondrule mineral (PCM) line (initially defined by chondrules from the Acfer 094 primitive carbonaceous chondrite), with most objects clustering at the intersection of the PCM line with the terrestrial fractionation (TF) line, near whole rock E3. The data from EH3 and EL3 overlap and show a similar distribution, suggesting they formed from a similar pool of precursors or in similar gaseous environments, but their mineral compositions suggest differences in their nebular environments and/or parent bodies. Silicates in the metal-rich nodules we analyzed (in both EH3 and EL3) have oxygen isotope ratios (as well as mineral compositions) similar to the silicate (metal-free) chondrules. This is consistent with formation of the metal-rich nodules prior to chondrite accretion, in an environment and from a process similar to that which formed the coexisting chondrules, but from more metal-rich mixtures of precursors. Olivine in an AOA from ALH 81189 is ^{16}O-rich with $\delta^{18}O = -46.5‰$, $\delta^{17}O = -48.0‰$, similar to the AOAs and refractory inclusions previously reported in E3 and in all other chondrite groups. There is a clear distinction in oxygen isotopic compositions between the chondrules in the E3 chondrites and those in the LL and R as well as those in CV and CM chondrite groups. Chondrules from CR and E chondrites plot closer to the PCM line than all other chondrite groups with E3 chondrules having a different distribution toward more ^{16}O-poor compositions. Chondrules in other chondrite groups form trends above and below the PCM. From the distribution of EC chondrules along the PCM line, we propose that similar pools of chondrule precursors were present in the different (carbonaceous, CR and Acfer 094 and non-carbonaceous, E) chondrule forming regions in the protoplanetary disk but with different amounts of ^{16}O-rich refractory materials, prior to development of the postulated *Jupiter divide* that potentially separated inner (non-carbonaceous) from outer (carbonaceous chondrite) Solar System materials or Jupiter was inefficient in completely separating these materials.

Keywords: Oxygen isotopes; Chondrite; Enstatite chondrite; EH3; EL3; Petrology; Chondrule

E-mail address: mweisberg@kbcc.cuny.edu (M.K. Weisberg)

https://doi.org/10.1016/j.gca.2021.02.027
0016-7037/

1. INTRODUCTION

Enstatite chondrites are important for constraining conditions and processes in the protoplanetary disk and they may be our closest examples of the material that accreted to form the terrestrial planets (e.g., Javoy 1995, 2010; Dauphas, 2017). They are among the most reduced solar system materials as indicated by their unique mineral assemblages and compositions (e.g., Keil, 1968; Weisberg and Kimura, 2012). Their whole rock stable (O, Cr, Ti, Ni and Zn) isotopic compositions are markedly similar to those of the Earth-Moon system (Javoy, 1995; Warren, 2011; Paniello, 2012), but Si isotopes differ, possibly supplying evidence against a direct relationship between E chondrites and the Earth -Moon system (Fitoussi and Bourdon, 2012; Savage and Moynier, 2013; Kadlag et al., 2019). However, metal-silicate Si isotope fractionation in a reduced nebular environment and vapor loss of lighter Si isotopes during planetary volatilization may have contributed to differences in the Si isotopic compositions between Earth and the E chondrites (Sikdar and Rai, 2020). It was recently shown that H, C and N isotopic compositions of E chondrites are also similar to Earth (Piani et al., 2020; Gray et al., 2021) and that enstatite chondrites contain enough H to have delivered to Earth three times the amount of water currently in its oceans. (Piani et al., 2020). The surface chemistry of Mercury suggests reduced E chondrite-like precursors (e.g., Nittler et al., 2011; Burbine et al., 2002; Ebel and Stewart, 2018). Thus, the E chondrites may be similar to the materials that were present in specific feeding zones during accretion of the terrestrial planets.

We previously studied the petrology and oxygen isotopic compositions of chondrules in the Sahara 97096, Yamato 691, Kota Kota and LEW 87223 E3 chondrites and showed that they define a slope ~1 line, termed the enstatite chondrite mixing (ECM) line (Weisberg et al., 2010, 2011), which is indistinguishable from the primitive chondrule mineral (PCM) line defined by Acfer 094 chondrules (Ushikubo et al., 2012). Here we report new, high precision, *in situ* oxygen isotopic analyses of 31 objects (chondrules, refractory inclusions and metal-rich nodules) in the highly primitive Allan Hills (ALH) 81189 (and paired ALH 85159) EH3 and, to our knowledge, the first oxygen isotopic analyses of individual objects in an EL3 chondrite, MacAlpine Hills (MAC) 88136. The goals of this work are to study the micro-distributions of oxygen isotopic compositions in chondrules and other objects in the most primitive EH3 and EL3 chondrites, further test the relationship between enstatite chondrite precursors and the precursors of other primitive chondrites (e,g., Acfer 094), explore the relationship between silicates among the different types of objects (including the reduced chondrules, metal-rich nodules, FeO-rich silicates and refractory inclusions) and better document and develop an understanding of the oxygen isotopic differences among the chondrules in primitive chondrites.

2. BACKGROUND

The distribution of three stable oxygen isotopes in chondrules at the micron scale has provided important insights into the process of isotope exchange between chondrule melt and surrounding gas (e.g., Yu et al., 1995; Boesenberg et al., 2005). *In situ* oxygen isotopic secondary ion mass spectroscopy (SIMS) analyses of chondrules in carbonaceous (C) chondrites has revealed the existence of ^{16}O-rich relict olivine grains (e.g., Yurimoto and Wasson, 2002; Jones et al., 2004; Kunihiro et al., 2004; Rudraswami et al. 2011; Ushikubo et al. 2012; Tenner et al., 2013; Marrocchi et al. 2018, 2019). However, excluding the minor occurrence of relict grains, minerals and glass in individual chondrules show indistinguishable oxygen isotope ratios (e.g., Ushikubo et al., 2012; Tenner et al. 2015), in contrast to earlier observations by Chaussidon et al. (2008) that reported pyroxene and mesostasis being ^{16}O-depleted in oxygen isotope ratios compared to olivine within the same chondrules. Reaction of chondrules with SiO molecules during chondrule formation has also been proposed to explain petrologic features, such as mineralogical zoning in chondrules (pyroxene-rich shells) (e.g., Tissandier et al., 2002; Libourel et al., 2006), which are likely the result of chondrules forming in open systems with respect to major oxides (Nagahara et al., 2008; Libourel and Portail, 2018). Under open-system chondrule formation, oxygen isotope exchange would have occurred efficiently between chondrule melt and the ambient gas (containing SiO, H_2O, and CO molecules) and resulted in internally homogeneous oxygen isotope ratios in each chondrule (Kita et al., 2010; Ushikubo et al., 2012; Tenner et al., 2015; Marrocchi and Chaussidon, 2015). Tenner et al. (2015) presented a mass balance model involving ^{16}O-poor water ice and solid precursors to explain their observation of systematic changes in $\Delta^{17}O$ ($=\delta^{17}O - 0.52 \times \delta^{18}O$) with redox state of the chondrules in CR chondrites, which was further applied to chondrules in CV (Hertwig et al. 2018). Marrocchi and Chaussidon (2015) presented a model in which SiO molecules played a major role in controlling mass independent fractionation of oxygen isotopes among chondrules in carbonaceous chondrites. In the case of ordinary (O) chondrite chondrules, Kita et al. (2010) suggested that the chondrule-forming region contained two kinds of solid precursors, (1) ^{16}O-poor solid precursors and (2) ^{16}O-rich solid precursors derived from the same oxygen isotope reservoir as carbonaceous chondrites. These two sources were mixed efficiently among chondrules as a result of open system behavior during chondrule formation through interactions between the heated chondrules and the ambient gas.

For the enstatite chondrites, Clayton and Mayeda (1985) indicated that individual chondrules from EH3 chondrites form a distinct cluster on the oxygen 3-isotope diagram, not overlapping chondrules from O or C chondrites and scattering about a best-fit line of slope 0.7. In contrast, Tanaka and Nakamura (2017) reported a best-fit line with a slope of 1.27 from chondrules in EH3 and EH4 chondrites that include data from 6 individual chondrules in EH3. However, our previous results on chondrules in four E3 chondrites showed that the oxygen isotope ratios ($\delta^{18}O$, $\delta^{17}O$) of olivine and pyroxene in E3 chondrules have a wide range of values spanning as much as 10 ‰ in both $\delta^{18}O$ and $\delta^{17}O$. Some chondrules from EH3 chondrites

cluster around the terrestrial fractionation line near enstatite chondrite whole rock values, some chondrules overlap the ordinary chondrite field on the 3-isotope diagram and some extend toward more ^{16}O-rich compositions similar to C chondrite chondrules (Weisberg et al., 2011). Olivine in some E3 chondrules shows a wide range of Δ^{17}O values (−4‰ to +2‰) that form a mixing line parallel to but distinct from the carbonaceous chondrite anhydrous mixing (CCAM) line (e.g., Clayton and Mayeda, 1984). This E3 chondrule olivine line was defined as the enstatite chondrite mixing (ECM) line (Weisberg et al., 2011) but, as mentioned above, it coincides with the line defined by chondrules from Acfer 094 referred to as the PCM (primitive chondrule mineral) line by Ushikubo et al. (2012).

Another important issue regarding the E chondrites is the origin of the more oxidized components in E3 chondrites. FeO-bearing silicates in enstatite chondrites are relatively rare and apparently out of equilibrium with the more typical reduced (e.g., near-pure enstatite) mineral compositions (e.g., Lusby et al. 1987; Weisberg et al., 1994). Weisberg et al. (1994) showed that the FeO-bearing silicates are older than the FeO-poor silicates, marking a more oxidized pre-history for these meteorites. It has been suggested that these minerals were transported from ordinary chondrite source regions to the E chondrite accretion zones (Lin et al., 2002). However, the FeO-bearing pyroxene in E3 chondrites has oxygen isotope values similar to coexisting pure enstatite, suggesting it formed locally and was not transported from the ordinary or other chondrule-forming region (Kimura et al., 2003; Weisberg et al., 2011). Additionally, the petrologic setting of the FeO-bearing pyroxene (enclosed in enstatite) suggests that it predates the reduced, FeO-poor enstatite-rich mineral assemblages and implies that conditions were initially more oxidizing in the E3 chondrule-forming region and/or that the mixture of chondrule precursors for E chondrites was, at least in part, compositionally similar to chondrule precursors of other chondrite groups. This is supported by the oxidation states of Ti in silicates, which contain a mixture of Ti^{3+} and Ti^{4+} (Simon et al., 2016).

Weisberg et al. (2011) reported oxygen isotopic heterogeneity among mineral grains within some of the chondrules in E3 chondrites. They suggested that this implies incomplete melting of the chondrules, survival of minerals from previous generations of chondrules, and chondrule recycling or possibly open system behavior during chondrule formation. One chondrule contained a relict grain with an R chondrite-like oxygen isotopic composition. The presence of R chondrite-like oxygen in a large, possibly relict, olivine grain suggests limited mixing of materials from other reservoirs and/or close proximity of E, O and R chondrite precursors.

Interestingly, the relatively rare calcium-aluminum-rich inclusions (CAIs) in E3 chondrites have petrologic characteristics and ^{16}O-rich oxygen isotopic compositions similar to CAIs in other chondrite groups and appear to have formed in a different oxygen reservoir from the E3 chondrules (Guan et al., 2000; Fagan et al., 2001; Lin et al., 2003). This suggests that CAIs in all chondrite groups may all have formed in the same region and then been distributed to the accretion zones of the various chondrite groups. However, oxygen isotopes indicate that formation and distribution of chondrules and their precursors was more complicated, with chondrules from each chondrite group forming in their own separate regions, from distinct reservoirs, presumably representing different heliocentric distances or nebular epochs.

3. METHODS

We selected 22 objects (chondrules, fragments, metal nodules, refractory inclusions) from thin section ALH 81189, 3 (EH3), 9 objects from ALH 85159, 5 (paired with ALH 81189) and 13 objects from MAC 88136, 37 (EL3) for oxygen isotope analysis. Element maps for all sections, back-scattered electron (BSE) images of each object and major mineral compositions were collected using a combination of electron beam instruments.

Wavelength dispersive spectroscopic (WDS) maps of Si, Al, Mg, Ca, Fe, Ti, S, P, Na and Ni X-ray emission intensity of each thin section were generated with a Cameca SX100 electron microprobe (at the AMNH). These are "stage maps" (moving stage, stationary electron beam). Operating conditions were 15 kV accelerating voltage and 40 nA beam current, with a dwell time of 12 ms on one micrometer beam spots spaced 4–7 microns apart. Mineral compositions were determined on nominally 1 μm spots using the Cameca SX100 and JEOL Super Probe (at Rutgers) electron microprobes. Natural and synthetic standards were chosen based on the compositions of the minerals being analyzed. An accelerating potential of 15 keV and a sample current of 20 nA were used for silicates and 20 keV and 25 nA for metal. Counting times were 20 s on peak, and 10 s on background (off-peak) spectrometer positions. Relative uncertainties (2 sigma) based on counting statistics for major elements (Si, Fe, Mg) are calculated to be <2% and for Ti, Cr, Mn and Ca they are 10%, 10%, 9% and 5%, respectively. Data reductions were carried out using instrument software based on methods described by Pouchou and Pichoir (1991).

Oxygen isotopes of silicates were analyzed *in situ*, using the Cameca IMS 1280 secondary ion mass spectrometer at the WiscSIMS laboratory. The goal was to measure six grains (olivine and pyroxene) in each object, if grain size allowed, to achieve a representative average and to test for internal homogeneity within each chondrule or other object. The analytical procedure was similar to that described in Kita et al. (2010). A Cs^+ primary ion beam was focused to 12 μm diameter at 2 nA. Secondary oxygen ions ($^{16}O^-$, $^{17}O^-$, and $^{18}O^-$) were detected simultaneously using multi-collector Faraday cups with three feedback resistors, 10^{10} ohm, 10^{12} ohm, and 10^{11} ohm for $^{16}O^-$, $^{17}O^-$, and $^{18}O^-$, respectively. As in previous studies, 16–25 unknown analyses were bracketed by 8 analyses of a San Carlos olivine reference material (SC-Ol; $\delta^{18}O = 5.32‰$; Kita et al., 2010). Two additional olivine, three pyroxene, and one quartz reference materials were also analyzed to correct instrumental bias (appendix). Average external reproducibility of bracketed SC-Ol analyses (2SD) was ~0.2 ‰ for $\delta^{18}O$ and 0.3 ‰ for $\delta^{17}O$ and $\Delta^{17}O$. The

external reproducibilities (2SD) for each bracket are assigned as the uncertainties of bracket unknown analyses.

4. RESULTS

4.1. Petrology

The objects we studied from ALH 81189 (Fig. 1a) and paired ALH 85159 (Fig. 1b) included 20 porphyritic pyroxene (PP), 1 PP with FeO-rich pyroxene, 2 porphyritic olivine-pyroxene (POP), 2 porphyritic olivine (PO), and 1 barred pyroxene chondrule; 1 amoeboid olivine aggregate (AOA); 1 diopside-plagioclase fragment; 2 isolated olivine fragments; and 1 metal-rich nodule containing enstatite (En_{98}). From MAC 88136 (Fig. 1c) we studied an unusually large (>1 mm) diopside-rich chondrule, a silica-pyroxene chondrule, a radial pyroxene (RP) and 7 PP chondrules, and 3 metal-rich nodules containing enstatite laths. The latter are the first oxygen isotopic data from silicates in metal-rich nodules in E3 chondrites.

As is typical of EH3 and EL3, most chondrules are dominantly FeO-poor enstatite and can be considered type IB (Fig. 2b, d). All textural types of Gooding and Keil (1981) are present in enstatite chondrites but (type I) porphyritic pyroxene (PP, e.g., Fig. 2b) is the most common type. Most of the PP chondrules we studied contain near-endmember enstatite ($En_{>98}$). One PP (C9) in ALH 81189 was dominated by FeO-rich pyroxene ($Wo_{0.1}En_{73\text{-}83}$) (Fig. 2c). Unlike most other chondrite groups, olivine is minor in the E3 chondrites. It occurs mainly as poikilitically enclosed grains in enstatite in the pyroxene-rich chondrules, but we also identified rare porphyritic olivine (PO) chondrules and relatively large, isolated olivine mineral fragments ($Fo_{>98}$) up to 300 μm in size in ALH 81189 (Fig. 2a).

Several unusual objects were also studied including a diopside–plagioclase chondrule (F9) in ALH 81189 unlike any chondrule or fragment previously described in any E3 chondrite. It is irregular in shape, ~300 μm across and composed mainly of laths of diopside ($Wo_{44.8}En_{54.3}$) having 2.5 wt.% Al_2O_3 and 1.5 TiO_2 and plagioclase ($An_{79.5}Ab_{20.5}$), with minor enstatite ($Wo_{0.6}En_{97.1}$) and silica (Fig. 3a). The AOA (F17) in ALH 81189 is an irregularly shaped inclusion consisting of olivine surrounding nodules of Ca-pyroxene and anorthite (Fig. 3b) and is texturally and mineral compositionally similar to AOAs in C chondrites (e.g., Grossman and Steele, 1976). The olivine has a composition of $Fo_{99.7}$, if calculated based on two end members (Fo and Fa). However, this olivine also contains 0.3 wt.% CaO.

The diopside-rich chondrule (C1) in MAC 88136 is ~50% coarse diopside ($Wo_{46.4}$ $En_{53.2}$) in thin section, occurring with enstatite ($Wo_{0.7}$ $En_{98.9}$), silica and troilite (Fig. 3c–d). Silica apparently occurs mainly along the edges of the diopside grains in the chondrule. The troilite in this chondrule contains 0.4 wt.% Ti and 0.4 Cr, as is typical of troilite in enstatite chondrites (e.g., Keil, 1968).

Metal nodules in EL3 chondrites (also called metal-silicate intergrowths) have been a subject of controversy as to whether they are primary, nebula-formed objects or products of impact melting. EH3 chondrites also contain metal-rich objects with assemblages of sulfides, phosphide, graphite and silicates (Lehner et al., 2010) and have been referred to as metal-sulfide nodules (MSN). The EL3

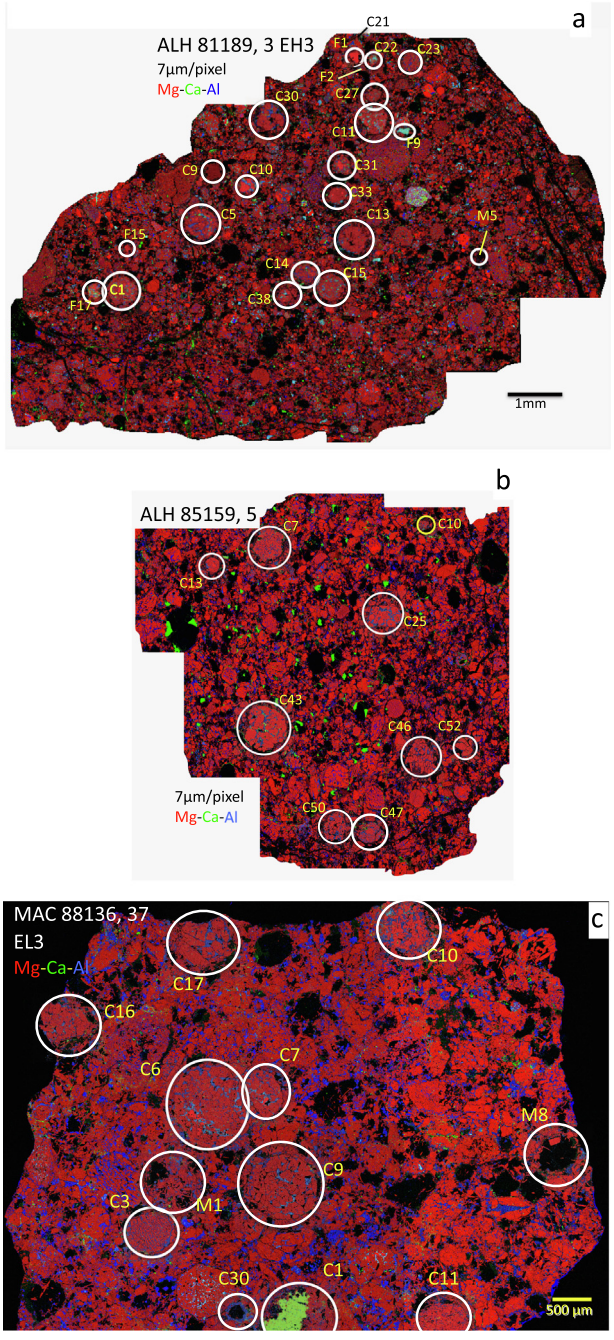

Fig. 1. Mg-Ca-Al (red–green-blue) element maps of the three unequilibrated enstatite chondrites studied: (a) ALH81189, 3 (b) ALH 85169, 5 and (c) MAC 88136, 37. The circled/numbered areas are the chondrules and other inclusions that were studied and analyzed for oxygen isotopes. On these maps the brightest reds are forsterite. The duller reds are enstatite which are the dominant silicate. Metal-sulfide-rich nodules appear mostly black. In (c) the green area marked C1 is the diopside-rich portion of the large chondrule CI in MAC 88136. Scale for 1a and 1b are the same. (For interpretation of the references to color in this figure legend, the reader is referred to the web version of this article.)

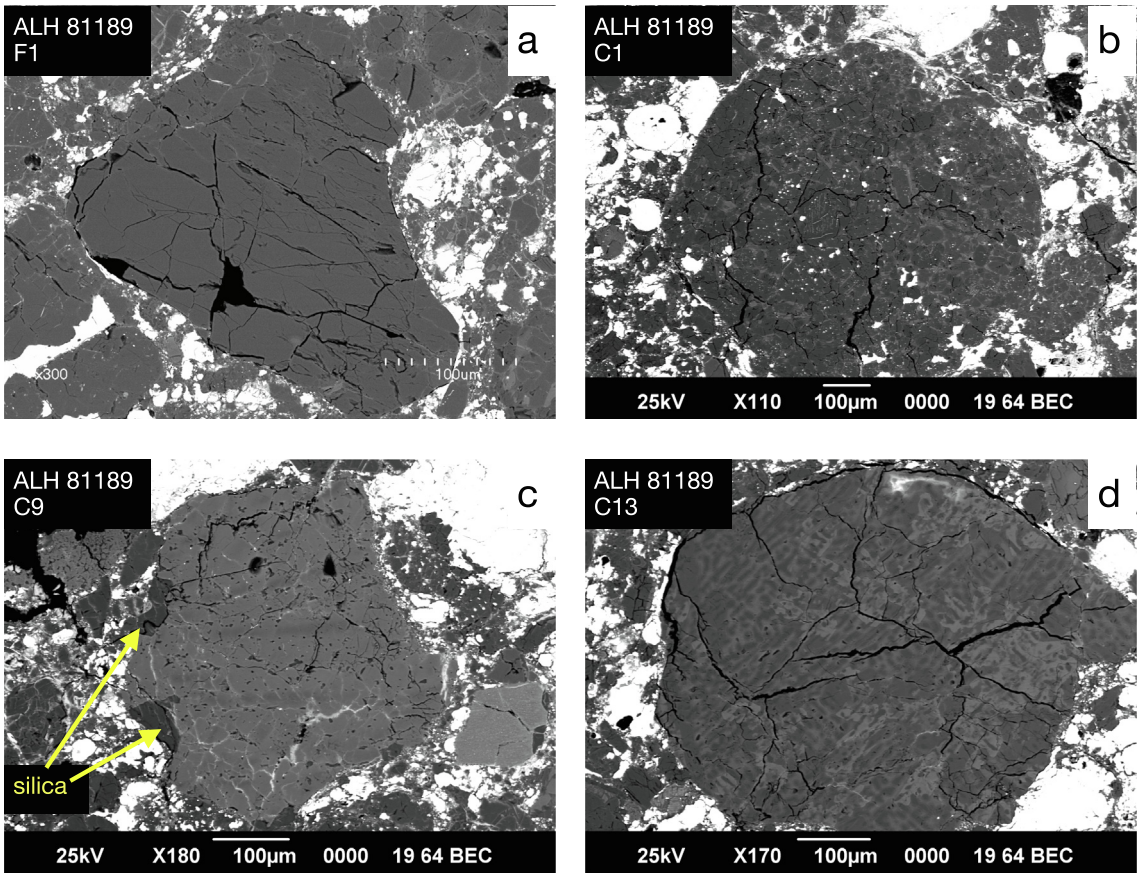

Fig. 2. Backscattered electron (BSE) images of representative chondrules and fragments in ALH 81189 that were analyzed for oxygen isotopes. (a) Olivine mineral fragment that is over 300 µm across. (b) Enstatite-rich chondrule containing minor forsterite, troilite and interstitial Na-Al-bearing mesostasis. This can be classified as a type IB porphyritic pyroxene chondrule and is representative of the chondrules that are common in E3 chondrites. (c) C9 is an irregular shaped object, possibly a broken chondrule, dominated by FeO-bearing pyroxene and minor silica. Such objects are rare in E3 chondrites. (d) C13 is a barred chondrule with larger grains (up to ~40 µm) of enstatite.

nodules contain laths of enstatite (~En_{98}) intergrown with metal. We studied one metal-rich nodule (M5) in ALH 81189 and three metal-rich nodules (M1-2, M8, and M10) in MAC 88136 (Fig. 4a-d). In the MAC 88136 EL3 chondrite, enstatite occurs mainly as laths, needles and irregular crystals within the metal. In the metal nodule in ALH 81189 studied here, the enstatite occurs as anhedral crystals oriented around metal in the center, forming what appears to be a discontinuous enstatite-rich layer (Fig. 4b).

Compositions of most silicates we analyzed are reduced enstatite (En > 98) and forsterite (Fo > 98) with a few exceptions such as C9 in ALH 81189 discussed above. Fig. 5 shows the distribution of silicate compositions in the sections studied.

4.2. Oxygen isotopes

Our new data for the average oxygen isotope ratios for each object we studied are given in Table 1 (complete dataset is in appendix) and plotted in Fig. 6 along with literature chondrule data from E chondrites. While whole rock E chondrites plot along the terrestrial fractionation (TF) line (e.g., Weisberg and Kimura, 2012), the majority of olivine and pyroxene analyses plot along the slope ~1 PCM line, with most data clustering at the intersection of the PCM with the TF line (Fig. 6a). The mean oxygen isotope ratios of individual chondrules were determined for most of the chondrules that show internally homogeneous oxygen isotopic ratios (Fig. 6b).

Two PP chondrules show a significant range of internal variability (Fig. 6c). ALH 81189 C1 contains ^{16}O-rich relict olivine grains that reach $\delta^{18}O$ and $\delta^{17}O \sim -30‰$, in contrast to those of pyroxene in the same chondrule that plot above the TF line. ALH 85159 C51 shows the highest $\delta^{18}O$ and $\delta^{17}O$ values among all of the chondrule studied and shows significant internal variability from 6‰ to 8‰ and from 4‰ to 6‰, respectively. Olivine in the AOA from ALH 81189 is ^{16}O-rich with $\delta^{18}O = -46.5‰$, $\delta^{17}O = -48.0‰$, similar to AOAs and refractory inclusions in other chondrite groups (Fig. 6c; e.g., Krot et al., 2004).

The individual chondrule data from ALH 81189 and ALH 85159 (EH3) and the more limited data set from MAC 88136 (EL3) overlap and show a similar distribution. The $\Delta^{17}O$ for ALH 81189 and paired ALH 85159 chondrules range from −1.4 to 1.3‰ and for MAC 88136 the range is slightly smaller at −0.6 to 1.3‰. Olivine-rich

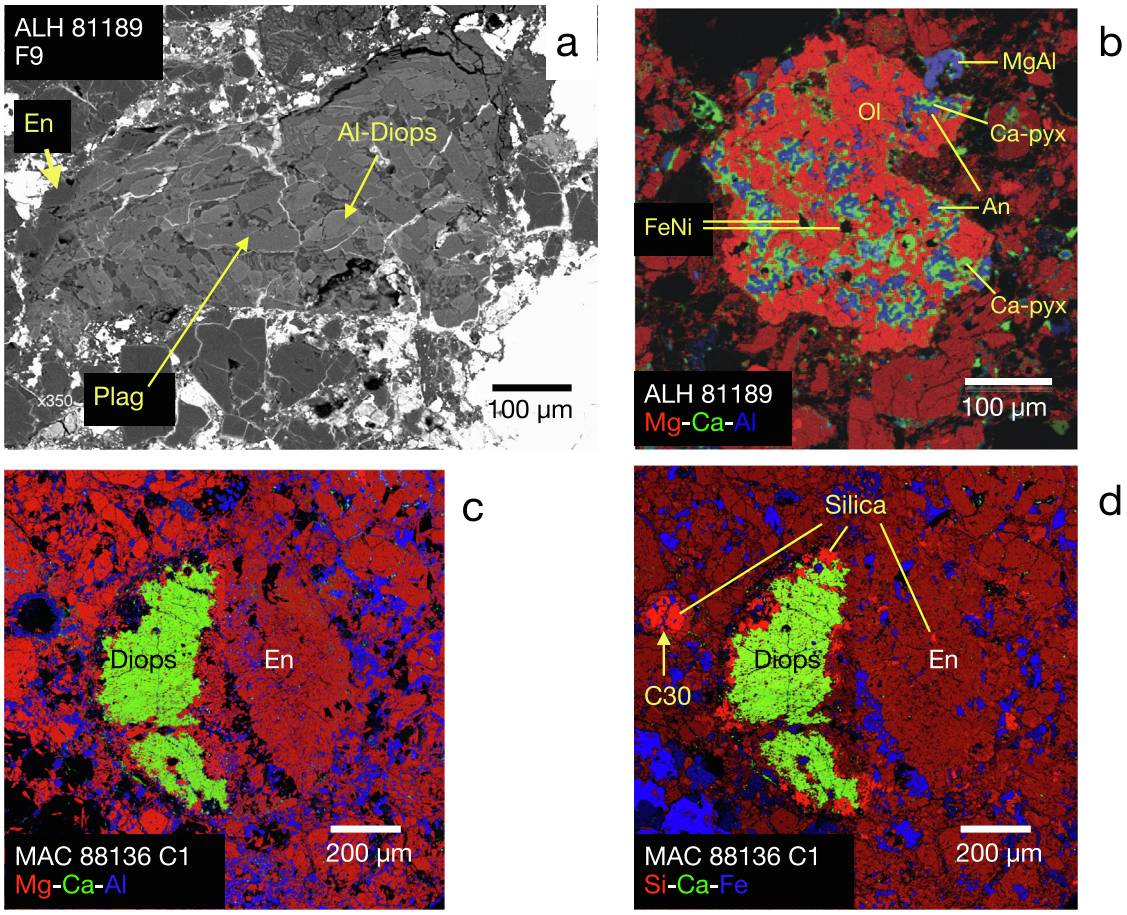

Fig. 3. Images of the more unusual objects identified in the E3 chondrites studied. (a) BSE image of a diopside-plagioclase inclusion in ALH 81189. (b) Mg-Ca-Al (red–green-blue, respectively) composite element map of an amoeboid olivine aggregate in ALH 81189 consisting of fine olivine surrounding inclusions (refractory nodules) composed of diopside (Ca-pyx), anorthite (An) and MgAl spinel (MgAl). (c) Mg-Ca-Al (red–green-blue) composite element map of C1 in MAC 88136, a large (~1mm) chondrule composed of diopside (Diops, green) and enstatite (En) with silica and Na-Al-rich plagioclase (blue). (d) Si-Ca-Fe (red–green-blue) composite element map of C1 showing that the silica (brigt red) occurs mainly around the edge of the diopside. Also shown is silica-rich chondrule C30. (For interpretation of the references to color in this figure legend, the reader is referred to the web version of this article.)

chondrules (PO, BO, POP) tend to plot on and below the TF line, while more PP chondrules plot above the TF line, as indicated from the distribution of individual olivine and enstatite data in Fig. 6a. The PP chondrule (C22) in ALH 81189 has the most ^{16}O-rich mean oxygen isotope ratios ($\delta^{18}O = 2.3‰$, $\delta^{17}O = -0.2‰$). Petrologically, C22 is a porphyritic pyroxene chondrule dominated by enstatite. The only petrologic difference between C22 and other chondrules in ALH 81189 is that C22 has a slightly higher amount of Al-rich mesostasis. The unusual diopside-rich chondrule in MAC 88136, and enstatite in the metal-rich nodules in both EH3 and EL3 all show oxygen isotopic ratios within a similar range of other chondrules. Silica from the silica-rich chondrule (C30) and the average of two analyses of silica in the diopside-rich chondrule (C1; Fig. 3c-d) in MAC 88136 are also plotted in Fig. 6b. They are compositionally similar, plotting on the TF line at $\delta^{18}O = 8.7‰$ and 8.3‰, respectively toward much more ^{16}O-poor compositions than olivine and pyroxene.

The data from most chondrules and other objects in ALH 81189, ALH 85159 and MAC 88136 form a regression line $\delta^{17}O = (0.88 \pm 0.10) \times \delta^{18}O - (2.1 \pm 0.5)$ that is statistically indistinguishable from the slope ~1 PCM line, $\delta^{17}O = (0.987 \pm 0.013) \times \delta^{18}O - (2.70 \pm 0.11)$ (Fig. 6d). Four chondrules from ALH 81189 and one from MAC 88136 appear to suggest a resolvable second trend above the PCM line (referred to as "other chondrules" in Fig. 6d). They show indistinguishable $\Delta^{17}O$ values ~0.9‰ (Fig. 6b) and may plot along the slope ~0.5 line (Fig. 6b). However, they comprise a linear trend with two heterogeneous chondrules, ALH 85159 C51 and three moderately ^{16}O-rich relict olivine grains from ALH 81189 C1 (Fig. 6d). A regression line through these data form a slightly shallower slope -0.84 ± 0.04 with an intercept of $-1.0 \pm 0.2‰$ (Fig. 6d). This second trend significantly overlaps with the chondrule data from LL chondrites (Kita et al. 2010). To check whether these two groups truly belong to two distributions in the two-dimensional space

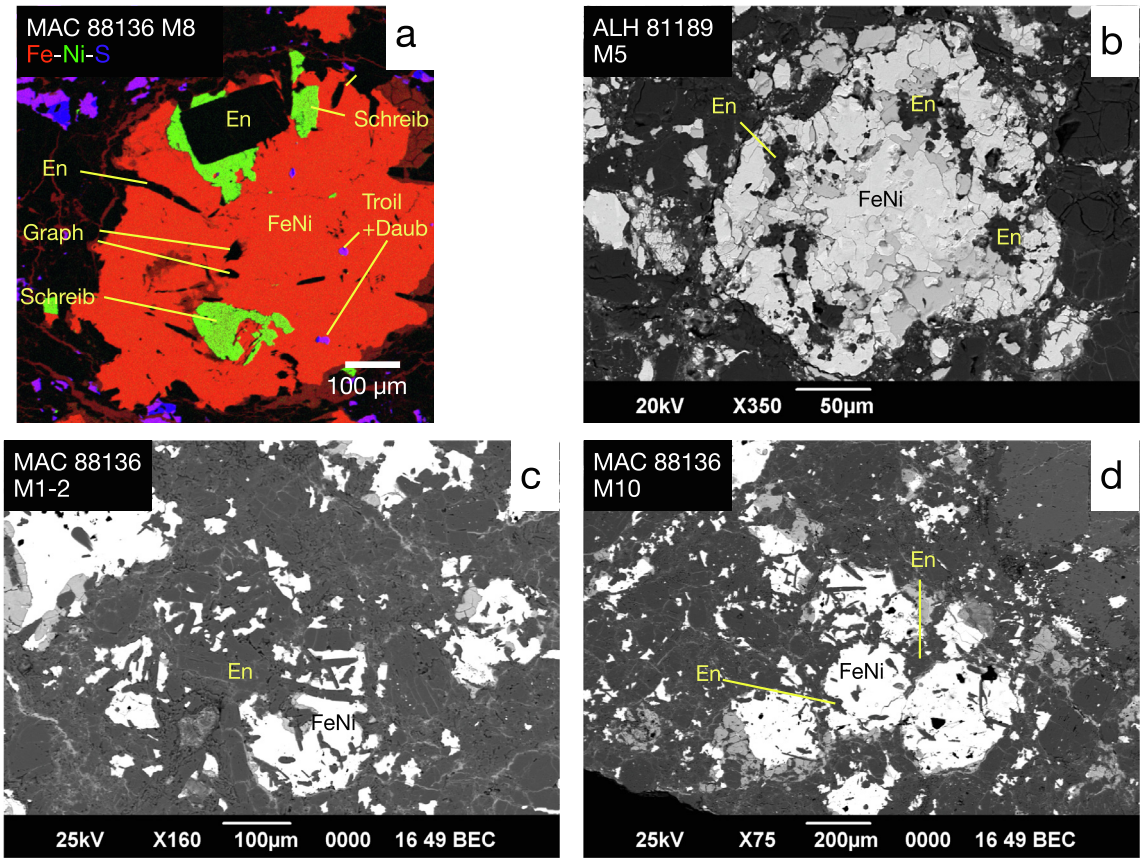

Fig. 4. Images of representative metal-rich nodules that were studied. (a) Fe-Ni-S (red–green-blue) composite element map of a nodule in MAC 88136 composed of schriebersite, graphite, troilite, daubreelite and enstatite surrounded by Si-bearing FeNi metal alloy (red). (b) BSE image of a metal-rich nodule in ALH 81189 composed of Si-bearing FeNi metal (white), troilite (medium grey) and enstatite (dark grey). (c) BSE image of a metal-rich nodule composed of Si-bearing FeNi metal intergrown with laths of enstatite. (d) BSE of a cluster of metal-rich nodules in MAC 88136 composed of Si-bearing FeNi (bright white), numerous enstatite laths (dark grey) and graphite (black). Oxygen isotopes were analyzed in the enstatite in all of these metal nodules. (For interpretation of the references to color in this figure legend, the reader is referred to the web version of this article.)

$\delta^{18}O$-$\delta^{17}O$, we performed a two-dimensional, two samples Kolmogorov-Smirnov test. This test is a non-parametric test that computes the probability that two samples belong to the same distribution by comparing their cumulative distributions. In this case, the test returns a P-value of 7.1×10^{-5}, well below the accepted threshold of 0.05 to reject the hypothesis, allowing us to conclude that these two trends are in fact two separate trends.

The data distribute in a similar range to those from our previous study of the Sahara 97096 and Yamato-691 EH3 and the anomalous LEW 87223 chondrite (Weisberg et al., 2011; Fig. 6e). The new dataset is also similar to the individual chondrule data reported by Clayton and Mayeda (1985) and Tanaka and Nakamura (2017), which are shown in Fig. 6e for comparison. In Fig. 6f, a regression line of all E3 chondrules is obtained by using these literature data and all data obtained in this study. The regression line gives $\delta^{17}O = (0.997 \pm 0.025) \times \delta^{18}O - (2.40 \pm 0.2)$, which is almost identical to the PCM line, but has a large MSWD of 24, reflecting two separate trends at the higher $\delta^{18}O$ and $\delta^{17}O$ ends.

Type I chondrules in some C chondrite groups show a trend of $\Delta^{17}O$ increasing with decreasing Mg# for type I chondrules, whereas such a trend is not observed for chondrules in O and R chondrites (Kita et al., 2010, 2015). The data for the E3 chondrules do not show a clear trend (Fig. 7). A regression line through the data ($r = 0.2$) shows a very slight hint of $\Delta^{17}O$ decreasing with the average Mg# for the chondrule silicates but it is not statistically significant.

5. DISCUSSION

5.1. Relationship between chondrules, metal-rich nodules and refractory inclusions in EH3 and EL3 chondrites

The oxygen isotopic compositions of the silicates within most chondrules analyzed in this study appear to be fairly uniform. Weisberg et al. (2011) specifically selected olivine-bearing chondrules and, as a result discovered oxygen isotopic heterogeneity in minerals from some individual chondrules in EH3 chondrites and suggested incomplete melting of the chondrules, survival of minerals from previous generations of chondrules, chondrule recycling, or possibly open system behavior during chondrule formation, as proposed for chondrules in O and C chondrites. Weisberg

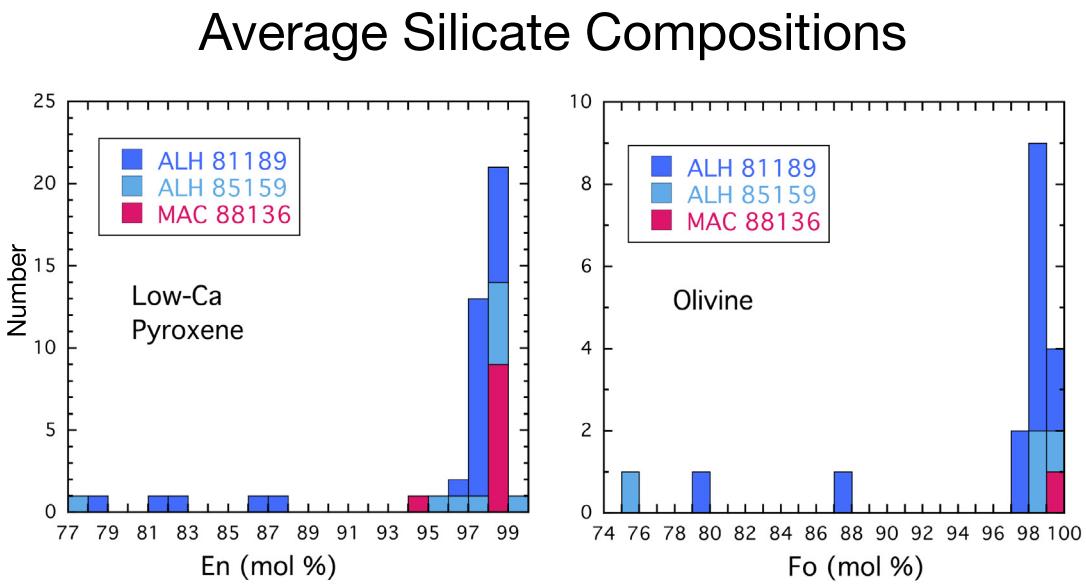

Fig. 5. Histograms showing the silicate compositions in the chondrules and other objects in the three E3 chondrites that were studied. As expected, all three E3 chondrites are dominated by enstatite (En) with near end-member composition. Most olivine is also near end-member forsterite (Fo). FeO-bearing silicates are much less common.

et al. (2011) found one chondrule in Sahara 97096 that contained an olivine grain with an R chondrite-like oxygen isotopic composition. They interpreted this to be a relict grain, suggesting limited mixing of materials from other reservoirs and the close proximity of E, O and R chondrite precursors, compared to C chondrites. This is consistent with recent discoveries of whole rock nucleosynthetic isotopic differences between non-carbonaceous (including E, O and R) and carbonaceous chondrites (Trinquier et al., 2009).

Overlap in oxygen isotopic compositions between EH3 and EL3 chondrules suggests that they share similar precursors but the mineral assemblages and compositions (e.g., higher Si content in EH metal) in EH3 and EL3 indicate different degrees of reduction (Keil, 1968; Weisberg and Kimura, 2012), suggesting differences in their nebular environments and/or separate, possibly multiple parent bodies (e.g., Weyrauch et al., 2018). Most of the components that we analyzed show similar oxygen isotopic compositions, including the chondrules and enstatite and forsterite mineral fragments, enstatite in metal-rich nodules and the silicates with more FeO-rich compositions. This is consistent with previous studies that showed that the less common FeO-bearing minerals in E3 chondrites share the same oxygen isotopic compositions as the more common, reduced, FeO-poor olivine and pyroxene in E3's (Weisberg et al., 2011, Kimura et al., 2003). Additionally, the unusual diopside-plagioclase fragment (F9; Fig. 3a) in ALH 81189 and the large diopside-enstatite chondrule (C1; Fig. 3c–d) in MAC 88136 also have similar isotopic compositions to the other E3 components. Thus, all of these objects likely formed from the same mix of precursors and were likely molten or partially molten and exchanged oxygen in the same, presumably chondrule-forming, region.

Derivation of the FeO-bearing silicates from the same oxygen reservoirs as the more reduced silicates and textural and compositional evidence indicating that the FeO-bearing silicates have undergone various degrees of reduction (Rambaldi et al. 1983; Lusby et al. 1987; Weisberg et al. 1994; Kimura et al. 2003; Weisberg et al. 2011), suggest a stage of more oxidizing conditions in the evolution of enstatite chondrites. This is consistent with studies of element valence states that also suggest E chondrites were originally more oxidized at some point in their history (e.g., Jacquet et al., 2015; Simon et al., 2016).

The origin of the metal-rich nodules in E3 chondrites has been controversial. There are four major, conflicting hypotheses for the origin of these nodules in EL3 chondrites: (1) the metal-rich nodules are products of impact melting and formed by mobilization and injection of metal into pores in the EL3 regolith (Van Niekerk and Keil, 2011), (2) metal-rich nodules are pre-accretionary and resulting from impact disruption of early differentiated bodies (Horstmann et al., 2014), (3) the nodules are chondrule-like melts formed in the early solar system (Weisberg et al., 2013; Ebel and Sack, 2013), and (4) the nodules are aggregates of condensates (El Goresy et al., 2017; Lin et al., 2011). Kadlag et al. (2019) measured Si isotopes in silicates and metal in an EH3 chondrite and showed differences in their Si isotopic compositions suggesting that the differences were inherited from different nebular reservoirs. However, Si isotope fractionation between silicate and metal may also be responsible for the differences. Based on major and trace element analyses, Lehner et al. (2014) concluded that the matrix, chondrule, and metal-sulfide nodule compositions are apparently complementary, suggesting all the components of the EH3 chondrites came from the same nebular reservoir.

The oxygen isotopic data can help shed light on the origin of the EL3 nodules. The nodules in the EL3 chondrites have irregular to near-spherical shapes and characteristi-

Table 1
Oxygen isotope ratios (‰) and uncertainties (Unc.) and average Mg#s for the chondrules studied from ALH 81189, ALH 85159 EH3 and MAC 88136 EL3 chondrites.

Meteorite	sample	Type	Phase	Avg. Mg#	N for mean	$\delta^{18}O$ (‰)	Unc.	$\delta^{17}O$ (‰)	Unc.	$\Delta^{17}O$ (‰)	Unc.
ALH 81189	C1	PP	En	99.3	5	6.08	0.46	3.96	0.28	0.80	0.13
ALH 81189	C5	PP	En	98.4	6	5.10	0.33	2.44	0.18	−0.21	0.12
ALH 81189	C9	PP	Pyx	81	6	4.34	0.34	1.76	0.23	−0.49	0.17
ALH 81189	C10	PO	Fo, En	98.3	6	5.08	0.32	2.38	0.18	−0.26	0.14
ALH 81189	C11	PP	Ol, En	98.7	6	5.17	0.35	3.53	0.31	0.85	0.22
ALH 81189	C13	Barred	Fo, En	99	6	4.41	0.35	1.64	0.27	−0.65	0.16
ALH 81189	C14	PP	En	98.9	6	5.23	0.32	2.45	0.25	−0.27	0.17
ALH 81189	C15	PP	En	98.8	6	5.34	0.32	2.72	0.26	−0.05	0.20
ALH 81189	C21	POP	Fo, En	98.8	4	4.73	0.39	2.35	0.27	−0.11	0.16
ALH 81189	C22	PP	En	99.3	4	2.33	0.50	−0.15	0.23	−1.36	0.16
ALH 81189	C23	PP	En	98.2	6	5.08	0.38	2.70	0.24	0.05	0.22
ALH 81189	C27	PP	En	99.1	1	6.40	0.40	4.13	0.28	0.81	0.21
ALH 81189	C30	PP	En	98.8	6	4.83	0.34	2.31	0.30	−0.20	0.20
ALH 81189	C31	POP	En	99.1	6	5.48	0.31	3.84	0.21	0.99	0.13
ALH 81189	C33	PP	En	98.1	6	5.30	0.36	2.78	0.23	0.03	0.16
ALH 81189	C38	PP	En	99.3	6	4.73	0.43	2.26	0.23	−0.20	0.14
ALH 81189	F1	Min Frag	Ol	98	4	4.86	0.32	2.35	0.22	−0.17	0.16
ALH 81189	F2	Min Frag	Ol	98.3	4	4.91	0.34	2.36	0.19	−0.19	0.18
ALH 81189	F5	PO	En	98.7	6	4.42	0.34	1.99	0.19	−0.31	0.12
ALH 81189	F9	Diops-plag	En	97.7	3	4.06	0.85	1.47	0.61	−0.64	0.19
ALH 81189	F17	AOA	Ol	99.7	2	−46.49	0.34	−47.98	0.24	−23.81	0.20
ALH 81189	M5	MN	En	98.5	4	4.44	0.43	2.09	0.30	−0.22	0.18
ALH 85159	C7	PP	En	99.1	6	5.77	0.65	3.25	0.35	0.25	0.12
ALH 85159	C13	PP	En	99.2	6	5.54	0.35	2.70	0.25	−0.18	0.18
ALH 85159	C25	PP	En	99.6	5	6.26	0.36	3.55	0.21	0.30	0.15
ALH 85159	C43	PP	En	99.8	6	5.97	0.35	3.18	0.20	0.08	0.16
ALH 85159	C46	PP	En	98.5	6	6.39	0.39	3.54	0.32	0.22	0.19
ALH 85159	C47	PP	En	99.4	6	6.57	0.40	3.76	0.19	0.34	0.13
ALH 85159	C50	PP	En	99.1	6	6.28	0.39	3.44	0.26	0.17	0.12
ALH 85159	C51	PP	En	99.3	6	6.85	0.78	4.84	0.61	1.27	0.24
ALH 85159	C52	PP	En	98.9	6	5.82	0.37	2.79	0.23	−0.24	0.18
MAC 88136	C1	Diops-rich	Diops/En	99.4	4	5.15	0.32	2.64	0.21	−0.04	0.16
MAC 88136	C1	Diops-rich	Silica		1	8.33	0.15	4.22	0.23	−0.12	0.25
MAC 88136	C1	Diops-rich	Silica		1	8.42	0.15	4.26	0.23	−0.12	0.25
MAC 88136	C3	PP	En	99.6	6	5.40	0.40	2.69	0.33	−0.12	0.19
MAC 88136	C6	PP	En	99.6	6	5.51	0.40	2.51	0.31	−0.35	0.20
MAC 88136	C7	PP	En	99.5	5	5.31	0.32	2.39	0.25	−0.38	0.21
MAC 88136	C9	PP	En	99.5	6	6.42	0.34	4.34	0.35	1.00	0.28
MAC 88136	C10	PP	En	99.6	6	5.45	0.35	2.94	0.38	0.11	0.30
MAC 88136	C11	RP	En	99.5	7	5.95	0.34	3.17	0.32	0.07	0.29
MAC 88136	C16	PP	En	99.0–99.9	6	5.93	0.34	3.10	0.25	0.01	0.20
MAC 88136	C17	PP	En	99.4	6	5.65	0.32	2.94	0.28	0.00	0.27
MAC 88136	C30	Silica-rich	Silica		1	8.73	0.15	4.55	0.23	0.01	0.25
MAC 88136	M1	MN	En	NA	4	5.55	0.35	2.81	0.24	−0.08	0.17
MAC 88136	M8	MN	En	98.8	2	5.81	0.38	3.07	0.27	0.05	0.19
MAC 88136	M10	MN	En	99.3	3	5.74	0.45	3.02	0.40	0.04	0.27

cally contain enstatite laths or needles intergrown with the metal (Fig. 4c and d). Their sharp boundaries with surrounding matrix and other objects suggest the nodules formed as free-floating objects similar to the chondrules. They may be aggregates of condensates or were molten or partially molten. For the limited number of metal-rich nodules we were able to analyze, the oxygen isotopic ratios (as well as the mineral compositions) of the enstatite laths in the metal-rich nodules are similar to those of enstatite in the silicate (metal-free) chondrules. Additionally, the metal-rich nodule and chondrule silicates all plot along the same (PCM) mixing line defined by the highly primitive Acfer 094 C chondrite. Although we cannot conclusively determine the origin of the metal-rich nodule silicates, the petrologic and oxygen data are more consistent with formation of the metal-rich nodules prior to chondrite accretion, in an environment similar to the coexisting chondrules, and forming from a process similar to that which formed the metal-free chondrules, but from more metal-rich mixtures of precursors.

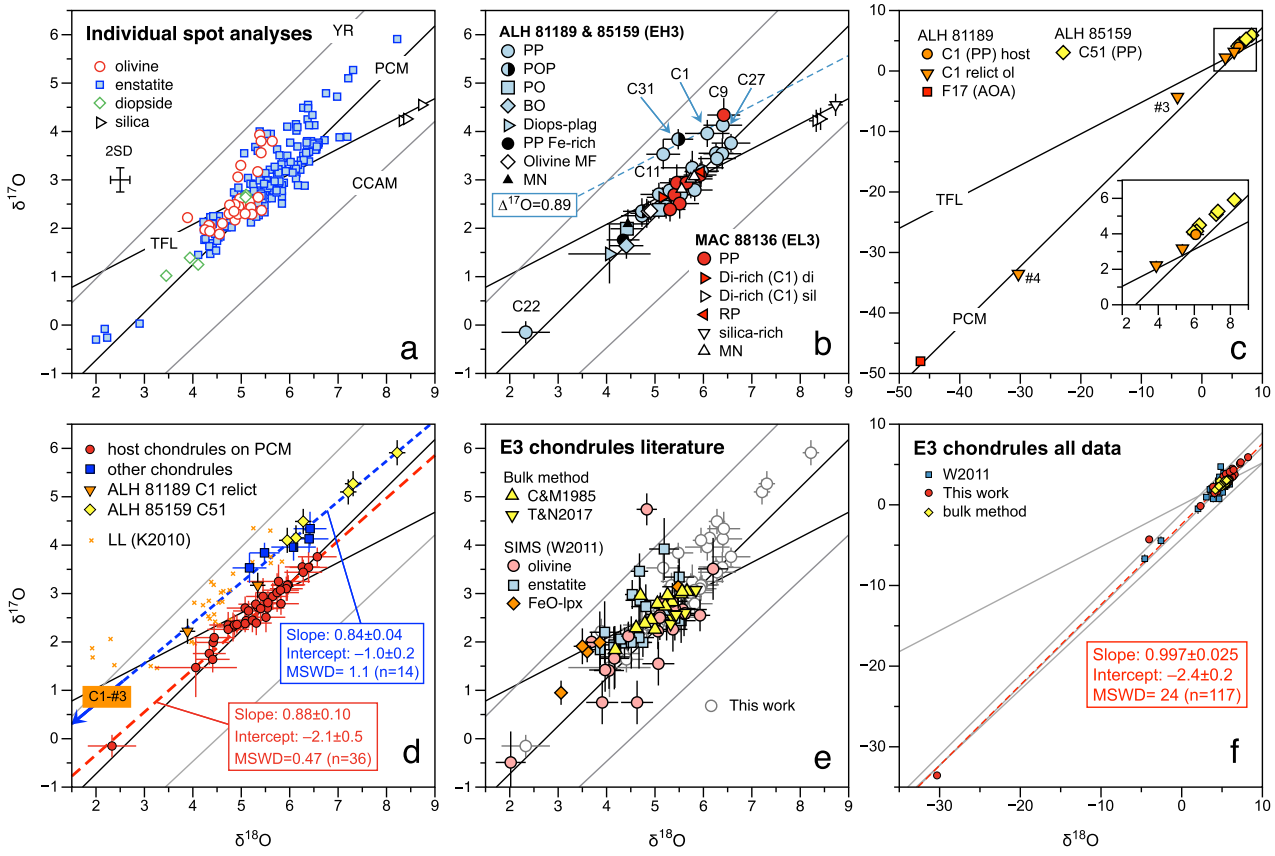

Fig. 6. Oxygen three-isotope ratios of chondrules in E3 chondrites. (a) Oxygen isotopic ratios of individual spot analyses. Data plot along primitive chondrule mineral (PCM) line (Ushikubo et al., 2012), but mostly clustering at its intersection with the terrestrial fractionation line (TF). Other lines are from Young and Russell (1998, Y-R), and the carbonaceous chondrite anhydrous mineral line (CCAM, Clayton and Mayeda, 1984). (b) Oxygen 3-isotope diagram showing average oxygen isotope ratios for each chondrule analyzed in ALH 81189, ALH 85159 and MAC 88136. A blue dashed line is drawn parallel to the PCM line through seven E chondrite objects that lie above the PCM, possibly forming a second trend. (c) Oxygen isotope ratios of the AOA in ALH 81189, relict olivine in ALH 81189 C1, and individual pyroxene analyses from ALH 85159 C51. Inset enlarges the data from ALH 85159 C51 and ALH 81189 C1 which plot above the TF line. (d) E3 chondrules are plotted in two groups; majority of chondrules that plot on the PCM line and *other chondrules* that plot along with relict olivine in ALH 81189 C1 and heterogeneous chondrule ALH 85159 C51. The regression lines (dashed lines) and MSWD of the fits of two groups are shown. Chondrule data from LL3 chondrites are shown for comparison. (e) Data from our previous work on other E3 chondrites (Weisberg et al., 2011) showing a similar trend with some chondrule olivine plotting toward more ^{16}O-rich compositions. E3 chondrules determined from bulk methods (C&M1985: Clayton and Mayeda, 1985; T&N2017: Tanaka and Nakamura, 2017) are also show, which generally agree within the range observed in our new dataset. (f) The regression line for all E3 chondrule data. Data used for estimating regression lines is shown in EA5. (For interpretation of the references to color in this figure legend, the reader is referred to the web version of this article.)

The separation of the metal and silicates in chondrites is not well understood. Metal-rich nodules may have been spatially or temporally separated from the metal-poor chondrules, possibly due to an aerodynamic or a magnetic sorting mechanism that resulted in local metal-rich and metal-depleted regions that contributed to the same parent body (e.g., Hubbard, 2016). Weisberg et al. (2013) suggested a fractional condensation model to account for earlier formed (higher temperature) metal-rich "chondrule" compositions. Metal condenses at higher temperatures (1375 K) than silicate (olivine, diopside and enstatite condense at 1100, 1050 and 950 K, respectively) in a nebular reservoir with a C/O ratio greater than 1 at 10^{-3} bar total pressure (Ebel, 2006, Plate 9). Thus, it is reasonable to consider the metal-rich nodules in E3 chondrites as essentially "metal-rich chondrules", as suggested by Gooding and Keil (1981) and Alpert et al. (2020) for ordinary chondrites.

5.2. The enstatite chondrite mixing line and the PCM line

Although the whole rock oxygen isotopic compositions for E chondrites plot along or close to the TF line on a three isotope diagram (Clayton and Mayeda, 1984, 1999; Weisberg et al., 2011; Weisberg and Kimura, 2012), the individual chondrules, mineral fragments and metal-rich nodules form a trend toward more ^{16}O-rich compositions, (Fig. 6a, b), consistent with our previous studies of chondrules in E3 chondrites (Weisberg et al., 2011). This trend is also supported by the findings of Tanaka and Nakamura (2017), though they suggested their data formed

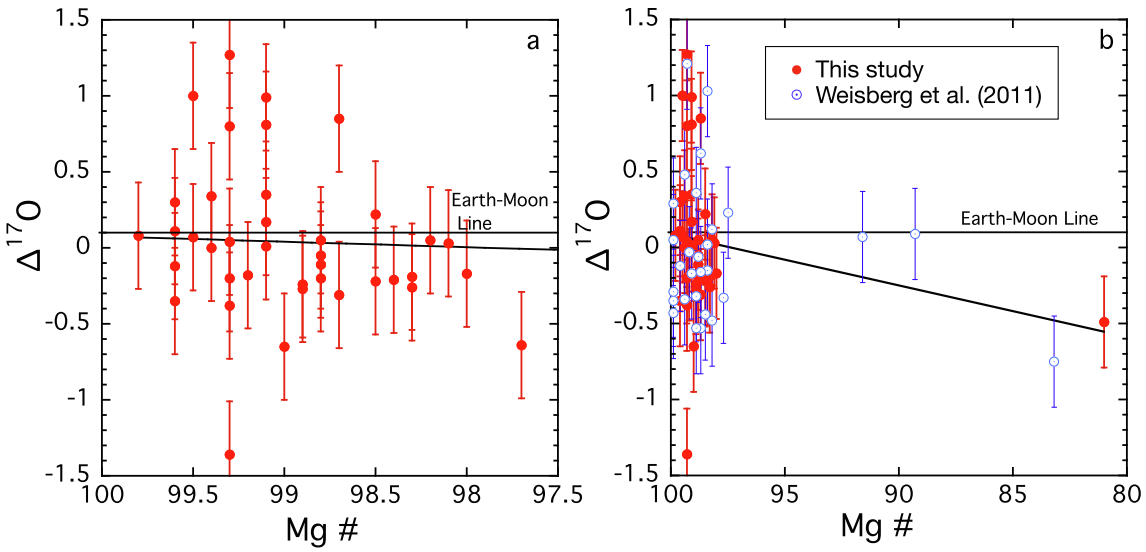

Fig. 7. (a) Average $\Delta^{17}O$ vs. average Mg# for the type I (FeO-poor) chondrules, fragments and metal-rich nodules in ALH 81189 EH3, paired ALH 85159 and MAC 88136 EL3 chondrites. (b) Average $\Delta^{17}O$ vs. average Mg# for all chondrules from this study and Weisberg et al. (2011). The lines are best fit lines through the data ($r = 0.2$). The AOA is not included.

a somewhat steeper slope. Weisberg et al. (2011) referred to the array of E3 chondrite oxygen isotopic ratios as the enstatite chondrite mixing line (ECM) but acknowledged that this mixing line is statistically indistinguishable from the slope-1 trend defined by chondrules from the primitive C chondrite Acfer 094 and referred to as the primitive chondrule mineral line (PCM) by Ushikubo et al. (2012).

Our data indicate a clear distinction between chondrules in the E chondrites and those in the LL chondrules which form a slope-0.5 trend mostly above the terrestrial fraction (TF) line with LL chondrules plotting to the left of the PCM (Kita et al., 2010). E chondrite chondrules differ from whole rock R chondrites which form a trend at even higher, ^{17}O-rich values (e.g., Bischoff et al., 2011) and R chondrite chondrules, which overlap with ordinary chondrite chondrules (Kita et al., 2015). The E3 chondrules are also isotopically different from CV and CM chondrite groups, which form a trend apparently parallel to but below the PCM line (Fig. 8). Chondrules from CR and EC chondrites plot closer to the PCM line than other chondrite groups (Fig. 8).

The PCM line is a regression line for individual SIMS olivine and pyroxene analyses from the Acfer 094 ungrouped C chondrite, including relict olivine and chondrules with internally heterogeneous oxygen isotopic ratios (Ushikubo et al., 2012). Chondrule data from other C chondrites generally plot on or near the PCM line (Rudraswami et al., 2011; Tenner et al., 2013, 2015; Marrocchi et al., 2018, 2019). The PCM line is interpreted to represent a mixing trend of two extreme primary oxygen isotope reservoirs of solids in the early solar system that potentially accreted to form the terrestrial planets, including the Earth (Ushikubo et al., 2012). It has been recognized that a small fraction of chondrules in carbonaceous chondrites, including Acfer 094, show OC-like oxygen isotopic ratios, which plot near the TF line ($\Delta^{17}O \sim 0‰$) but left of the PCM line

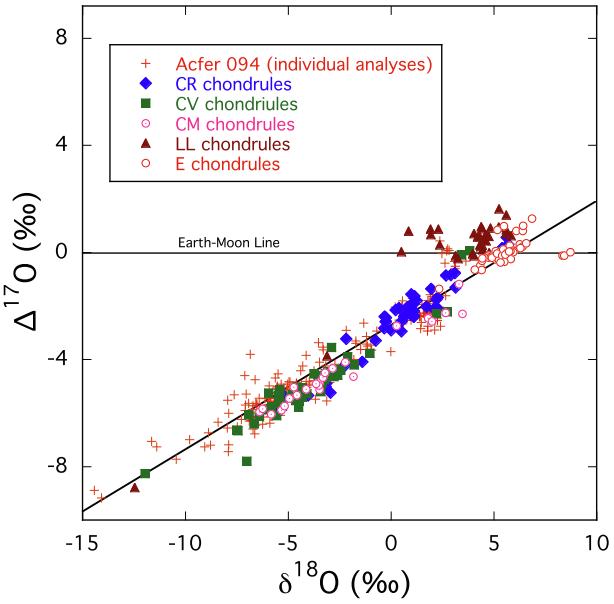

Fig. 8. Comparison of the chondrule oxygen isotope data for E chondrite chondrules to those in Acfer 094 and CR, CV and CM carbonaceous chondrites and LL ordinary chondrites. Data from this study, Ushikubo et al. (2012), Chaumard et al. (2018), Tenner et al. (2015), Hertwig et al. (2018, 2019b), Kita et al. (2010).

in oxygen three isotope space (Tenner et al. 2017; Hertwig et al. 2018, 2019a, 2019b). On the contrary, chondrule analyses from CV and CM chondrites (Hertwig et al. 2018, 2019b; Chaumard et al. 2018, 2021), which are with slightly better precisions compared to earlier studies, are offset slightly from the PCM line, to the right. Recently, Williams et al. (2020) observed that oxygen isotope ratios of CV chondrite chondrules show two linear trends that are related to their $\varepsilon^{50}Ti$ and $\varepsilon^{54}Cr$ abundances. Chondrules

with positive ε^{50}Ti and ε^{54}Cr plot with constant offset below the PCM line and chondrules with negative ε^{50}Ti and ε^{54}Cr plot towards OC chondrule compositions. These chondrule populations might have formed in the outer and inner protoplanetary disk, respectively. Thus, the PCM line might represent an average of the two trends found by Williams et al. (2020). Schneider et al. (2020) also reported ε^{50}Ti and ε^{54}Cr values of chondrules in several chondrite groups including CV, but did not find negative ε^{54}Cr anomalies from chondrules in CV. However, their CV chondrite chondrule data were limited to the dominant type I chondrules with negative Δ^{17}O. Kita et al. (2010) argued that condensation of olivine from high temperature gas could have resulted in deviation of oxygen isotopes to the left of the PCM line. Contribution of such fractionated precursors could have been much less abundant among the chondrule precursors for E chondrites than in other chondrite groups.

The distribution of chondrules along the PCM line is different between the E3 chondrules and the CR chondrules (Fig. 8). Chondrules from CR and Acfer 094 extend toward more ^{16}O-rich compositions (Ushikubo et al., 2012; Schrader et al., 2013, 2014, 2017; Tenner et al., 2015) while the E3 chondrules mainly form a tighter cluster of data points closer to the TF line (zero in Fig. 8) and E3 whole rock. One possible explanation for this difference is that the amount of ^{16}O-rich refractory material that was mixed into the E3 chondrule-forming region was less than that in the carbonaceous chondrite chondrule forming regions. This may be recorded in the very low abundance of CAIs and AOAs in the E3 chondrites (e.g., Guan et al., 2000; Fagan et al., 2001; Lin et al., 2003). Of the 3 thin sections studied, we found only one AOA. Additionally, this interpretation is supported by the relatively lower Ca/Si and Al/Si ratios of E chondrites relative to other chondrite groups (e.g., Hutchison et al., 2005), and their depletion in refractory lithophile trace elements (Dauphas and Pourmand, 2015). The suggestion of refractory material as chondrule precursors is also consistent with the findings of Jacquet and Marrocchi (2017) that chondrules show recognizable subdued group II REE patterns, presumably inherited from a refractory precursor.

Thus, we propose that a similar pool of chondrule precursors were distributed to the different (C, carbonaceous, and E, non-carbonaceous) chondrule forming regions in the protoplanetary disk but with different amounts of ^{16}O-rich refractory materials, prior to development of the postulated *Jupiter divide* (e.g., Warren, 2011; Kruijer et al., 2017). Such an interpretation would be consistent with recent measurements of individual chondrules in C chondrites (Williams et al., 2020). Williams et al. (2020) suggested the Jupiter barrier was inefficient allowing chondrules to move from the inner disk to the outer disk at 2–3 Ma after CAI formation. Additionally, Schrader et al. (2020) showed that dusty olivine chondrules in O and C chondrites have O-isotope compositions that match those of UOC chondrule olivine (Δ^{17}O $\sim$ 0‰), suggesting an origin from a UOC source. They suggested that UOC chondrules and/or chondrule fragments migrated from the inner Solar System outwards to CM chondrite chondrule-forming region, beyond the orbit of Jupiter.

Alternatively, the range of E3 oxygen isotopes could reflect addition of heavy isotopes in more volatile precursor material (e.g., cosmic symplectite and/or organic matters, Sakamoto et al., 2007; Hashizume et al. 2011). The Δ^{17}O values of non-carbonaceous chondrites correlates with the "oxygen excess" values calculated by the amounts of iron oxide and phosphates (Alexander et al., 2019) and a positive correlation was found for Δ^{17}O and Mg # for type I chondrules in CR chondrites (Tenner et al., 2015). These data suggest that the amount of H_2O may also be an important factor in controlling the Δ^{17}O values of chondrules. Thus, Δ^{17}O of chondrules in carbonaceous chondrite groups may be partially controlled by interaction with water. However, E chondrites have relatively low abundances of H_2O and do not show a positive relationship between Mg# and Δ^{17}O, as in the carbonaceous chondrites.

The trend in E3 chondrule oxygen has also been interpreted to result from reactions between ^{16}O-rich, olivine-rich chondrule melts and ^{16}O-poor SiO-rich gas (Tanaka and Nakamura, 2017). Tanaka and Nakamura (2017) suggested that such reactions may explain the oxygen isotopic systematics, by adapting the model presented by Marrocchi and Chaussidon (2015), as well as the reduced and silica-saturated compositions of E chondrite chondrules. They reported a slope of 1.27 for their oxygen isotopic compositions. In the Marrocchi and Chaussidon (2015) model, the systematic oxygen isotopic variations in C chondrite chondrules result from open-system gas–melt exchanges during chondrule formation. In their model, the PCM line does not correspond to a mixing line between two discrete reservoirs but instead records the signature of high-temperature interactions between nebular gas and dust (of CI composition and plotting on the carbonaceous chondrite anhydrous mineral [CCAM] line) produced in the accretion disk. Tanaka and Nakamura (2017) used the same model with slightly different endmember oxygen isotope ratios to explain the observed EH3-4 chondrule data that plot along the line with the slope >1. However, the slope-1.27 line estimated by Tanaka and Nakamura (2017) is based on data that includes enstatite chondrites more equilibrated than type 3. For their unequilibrated chondrites (EH3), they report 6 individual chondrules and 13 data points that are from composite chondrules or enstatite separates. A regression line through their unequilibrated chondrite data, the EH3 data from Weisberg et al., (2011) and our new data here are not distinguishable from a slope-1 line.

Gas-melt interactions during chondrule formation has been cited as a major factor in producing the petrologic features of chondrules (Ebel et al., 2018). Marrocchi and Libourel (2013) argued that the sulfur content of chondrules is dependent on the fS_2 and fO_2 of the surrounding gas. Using cathodoluminescence (CL) Libourel and Portail (2018) documented internal zoning of chondrule olivine and interpreted it as evidence for high-temperature gas-assisted near-equilibrium epitaxial growth of the olivine during chondrule formation. Jacquet et al., (2021) identified CL zoning in isolated olivine grains as a signature of decreasing refractory element concentrations toward the margins of grains, and took it to be evidence of interaction of the grains with the surrounding gas. For enstatite

chondrites, Piani et al. (2016) suggest that most of the sulfides found in EH3 chondrite chondrules are magmatic minerals that formed after the diffusion of S from a volatile-rich gaseous environment into the molten chondrules. Additionally, sulfidation of silicates has been proposed as the mechanism for formation of Niningerite in EH3 chondrites (e.g., Rubin 1983; Lehner et al., 2013). Thus, open system behavior may have also played a role in establishing the oxygen isotopic compositions of E3 chondrules.

In the oxygen isotope exchange model proposed by Marrocchi and Chaussidon (2015) for carbonaceous chondrites, they consider evaporation of CI chondritic dust that contains much more C and H compared to E chondritic materials. If the ambient gas during E chondrite chondrule formation was depleted in H_2O and CO molecules and enriched in SiO, gas–melt oxygen isotope exchange would produce negligibly small mass dependent fractionation in chondrule melts, due to small equilibrium fractionation between silicate and SiO gas (e.g., 0.39‰ at 1600 K between pyroxene and SiO gas; Javoy 2012). This is consistent with the observed slope ~1.0 regression line determined from the E3 chondrule data presented in Fig. 6f.

5.3. A second trend?

Data from seven of the chondrules analyzed here form a separate trend above the PCM line. These oxygen isotopic compositions overlap those of some OC chondrules (Kita et al., 2010) but extend toward more ^{16}O-poor compositions (Fig. 6d). These chondrules have reduced (Mg-rich) silicate compositions and are petrologically similar to other chondrules in ALH 81189. The trend may be the result of limited mixing between the different oxygen reservoirs. Substantial overlap between the second group chondrule data and LL chondrite chondrules (Fig. 6d) may suggest some mixing of OC-like precursors in E chondrite forming regions. Weisberg et al. (2011) found enstatite in Sahara 97096 with oxygen isotopic ratios that plotted within the field for ordinary chondrite chondrules and a relict grain within a chondrule that had a ^{17}O-rich composition similar to R chondrites. They concluded that there was transport and some mixing of the materials thought to have formed inside of Jupiter, i.e., the O, R and E chondrite reservoirs.

5.4. Significance of the oxygen isotopic composition of silica

The common occurrence of silica in chondrules and Si in metal in enstatite chondrites, a result of their silica-saturated compositions, is one of the characteristic features that distinguish E chondrites from the other chondrite groups. Silica grains from two different objects (a silica-rich and a diopside-rich chondrule) in MAC 88136 are isotopically similar, plotting on the TF line at $\delta^{18}O = 8.7‰$ and 8.3‰, respectively, and have different oxygen isotope compositions than the olivine and pyroxene in the same chondrules (Fig. 6b). Additionally, the silica plots further up the TF line relative to whole rock compositions (Fig. 6a, b). Thus, they potentially mass balance the more ^{16}O-rich compositions of some chondrules to yield the whole rock composition.

Kimura et al. (2005) studied silica polymorphs as a mechanism to understand the thermal histories of E chondrites. They reported cristobalite and tridymite in chondrule mesostases consistent with silica as the liquidus phase after crystallization of enstatite, and consistent with melting and rapid crystallization rates for the chondrules. As the last crystallizing phase, silica may have exchanged oxygen with and preserved the composition of the ambient nebular gas. It is also possible that silica condensed from a late stage SiO-rich nebular gas as suggested for silica-rich rims on some chondrules in CR chondrites (Krot et al., 2004). The silica could also form by reduction of Fe from FeO-bearing silicates as observed in some chondrules in unequilibrated E chondrites (e.g., Weisberg et al., 1994). However, FeO-bearing silicates have oxygen isotopic compositions similar to enstatite and forsterite in the chondrules (e.g., Kimura et al., 2003). Thus, reduction reactions would not explain the observed oxygen isotopic compositions of the silica.

In the case of MAC 88136 C1, the $\Delta^{17}O$ of the silica grains are indistinguishable from those of pyroxene in the same chondrule, but the $\delta^{18}O$ of silica grains are ~3‰ higher than pyroxene, which corresponds to a temperature of equilibrium at 600–700 °C using oxygen isotope thermometry (Clayton and Kieffer, 1991; Javoy et al., 2012). However, this temperature seems to be too low if the silica is a high temperature polymorph (as found for chondrule silica by Kimura et al., 2005). Alternatively, silica acquired higher $\delta^{18}O$ during low temperature parent body heating because of its fast oxygen isotope diffusion rate compared to olivine and pyroxene (e.g., Cole and Chakraborty, 2001). The difference in $\delta^{18}O$ may also be the result of applying the instrumental bias of quartz to correct for cristobalite. The difference in bias between quartz and cristobalite has not been evaluated but the $\Delta^{17}O$ values are not affected (Ushikubo et al., 2012).

6. CONCLUSIONS

1) The oxygen isotopic compositions of the silicates in most of the E3 chondrules are fairly uniform within each chondrule, with a few exceptions.
2) The oxygen isotopic compositions in EH3 and EL3 chondrules overlap, suggesting that they share similar precursors but the mineral assemblages and compositions in EH3 and EL3 indicate different degrees of reduction (e.g., Keil, 1968; Weisberg and Kimura, 2012), suggesting differences in their nebular environments and/or separate, possibly multiple (e.g., Weyrauch, et al., 2018), parent bodies.
3) The limited metal-rich nodules we analyzed have oxygen isotopic ratios (as well as mineral compositions) similar to the silicate (metal-free) chondrules. This is consistent with formation of the metal-rich nodules prior to chondrite accretion, in an environment similar to the coexisting chondrules, and their

forming from a process similar to that which formed the metal-free chondrules, but from more metal-rich mixtures of precursors.

4) Our data indicate a clear distinction between chondrules in the E chondrites and those in the LL or R chondrules. E chondrite chondrules also differ from CV and CM chondrite groups, which form a trend parallel to but below the PCM line. The chondrules from CR and E3 chondrites plot closer to the PCM line than all other chondrite groups.
5) The distribution of chondrules along the PCM line is different between the E3 chondrules and the CR chondrules, with CR chondrules extending toward more ^{16}O-rich compositions (Schrader et al., 2013, 2014, 2017; Tenner et al., 2015) while the E3 chondrules mainly form a tighter cluster of data points closer to the TF line near E3 whole rocks. A possible explanation is that a smaller amount of ^{16}O-rich, refractory material was mixed into the E3 chondrule-forming region than that into the carbonaceous chondrite chondrule-forming regions. Thus, we propose that similar pools of chondrule precursors were distributed to the different (C, carbonaceous, and E, non-carbonaceous) chondrule forming regions in the protoplanetary disk but with different amounts of ^{16}O-rich refractory materials, prior to development of the postulated *Jupiter divide* (e.g., Warren, 2011; Kruijer et al., 2017) and/or Jupiter was inefficient in separating these materials (e.g., Williams et al., 2020).
6) Data from seven of the EC chondrules analyzed appear to form a separate trend above the PCM line.
7) The PCM line might represent an average of the two oxygen isotope trends that Williams et al. (2020) observed in CV chondrules, which they related to their ε^{50}Ti and ε^{54}Cr abundances. Kita et al. (2010) argued that condensation of olivine from high temperature gas could have resulted in deviation of oxygen isotopes to the left of the PCM line. Contribution of such fractionated precursors could have been much less significant among the chondrule precursors for E chondrites, explaining why the EC chondrules plot closer to the PCM line than some of the other chondrite groups.

Declaration of Competing Interest

The authors declare that they have no known competing financial interests or personal relationships that could have appeared to influence the work reported in this paper.

ACKNOWLEDGEMENT

This material is based upon work partially supported by the National Aeronautics and Space Administration under grants #80NSSC18K0589 (MKW), and NNX16AD37G (DSE) issued through the Emerging Worlds program. AMNH staff provided invaluable assistance, including M. Chase, A. Smith, and C. Martin and Kingsborough CUNY staff including Robert Schenck. WiscSIMS is partly supported by NSF (EAR 1658823).

APPENDIX A. SUPPLEMENTARY MATERIAL

Supplementary data to this article can be found online at https://doi.org/10.1016/j.gca.2021.02.027.

REFERENCES

Alexander C. M. O'D. (2019) Quantitative models for the elemental and isotopic fractionations in the chondrites: the non-carbonaceous chondrites. *Geochim. Cosmochim. Acta* **254**, 246–276.

Alpert S. P., Ebel D. S., Weisberg M. K. and Neiman J. (2020) Petrology of the opaque assemblages in unequilibrated ordinary chondrites. *Meteorit. Planet. Sci.*. https://doi.org/10.1111/maps.13619, in press.

Bischoff A., Vogel N. and Roszjar J. (2011) The Rumuruti chondrite group. *Chem. Erde* **71**, 101–133.

Boesenberg J. S., Young E. D., Ziegler K. and Hewins R. H. (2005) Evaporation and the absence of oxygen isotopic exchange between silicate melt and carbon monoxide gas at nebular pressures. *Meteorit. Planet. Sci. Suppl.* **40**, A22.

Burbine T. H., McCoy T. J., Nittler L. R., Benedix G. K., Cloutis E. A. and Dickenson T. L. (2002) Spectra of extremely reduced assemblages: implications for Mercury. *Meteorit. Planet. Sci.* **37**, 1233–1244.

Chaumard N., Defouilloy C. and Kita N. T. (2018) Oxygen isotope systematics of chondrules in the Murchison CM2 chondrite and implications for the CO-CM relationship. *Geochim. Cosmochim. Acta* **228**, 220–242.

Chaumard N., Defouilloy C., Hertwig A. T. and Kita N. T. (2021) Oxygen isotope systematics of chondrules in the Paris CM2 chondrite: Indication for a single large formation region across snow line. *Geochim. Cosmochim. Acta* **229**, 199–218.

Chaussidon M., Libourel G. and Krot A. N. (2008) Oxygen isotopic constraints on the origin of magnesian chondrules and on the gaseous reservoirs in the early Solar System. *Geochim. Cosmochim. Acta* **72**, 1924–1938.

Clayton R. N. and Kieffer S. W. (1991) Oxygen isotopic thermometer calibrations. *Geochem. Soc., Spec. Publ.* **3**, 3–10.

Clayton R. N. and Mayeda T. K. (1984) Oxygen isotopic compositions of enstatite chondrites and aubrites. *J. Geophys. Res.* **89**, C245–C249.

Clayton R. N. and Mayeda T. K. (1985) Oxygen isotopes in chondrules from enstatite chondrites: possible identification of a major nebular reservoir (abstract). *16th Lunar and Planetary Science Conference 142–143*.

Clayton R. N. and Mayeda T. K. (1999) Oxygen isotope studies of carbonaceous chondrites'. *Geochim. Cosmochim. Acta* **63**, 2089–2104.

Cole D. R. and Chakraborty S. (2001) Rates and mechanisms of isotopic exchange. *Rev. Mineral. Geochem.* **43**, 83–223.

Dauphas N. (2017) The isotopic nature of the Earth's accreting material through time. *Nature* **541**, 521–524.

Dauphas N. and Pourmand A. (2015) Thulium anomalies and rare earth element patterns in meteorites and Earth: nebular fractionation and the nugget effect. *Geochim. Cosmochim. Acta* **163**, 234–261.

El Goresy A., Lin Y., Miyahara M., Gannoun A., Boyet M., Ohtani E., Gillet P., Trieloff M., Simionovici A., Feng L. and Lemelle L., et al. (2017) Origin of EL3 chondrites: Evidence for

variable C/O ratios during their course of formation—A state of the art scrutiny. *Meteorit. Planet. Sci.* **52**, 781–806.

Ebel D. S. (2006) Condensation of rocky materials in astrophysical environments. In *Meteorites and the Early Solar System II* (eds. D. Lauretta and H. Y. McSween). University Arizona, Tucson, pp. 253–277.

Ebel, D. S., Alexander C. M. O'D. and Libourel G. (2018) Vapor-melt exchange - Constraints on chondrule formation conditions and processes. In Chondrules: Records of Protoplanetary Disk Processes. Eds. S. Russell, A. Krot and H. C. Connolly Jr. Cambridge U. Press. pp. 151–174.

Ebel D. S. and Sack R. O. (2013) Djerfisherite: Nebular source of refractory potassium. *Contrib. Miner. Petrol.* **166**, 923–934.

Ebel D. S. and Stewart S. T. (2018) The elusive origin of Mercury. In *Mercury: The View after MESSENGER* (eds. C. Solomon, B. J. Anderson and L. R. Nittler). Cambridge University Press, Cambridge, pp. 497–515.

Fagan T., McKeegan K. D., Krot A. N. and Keil K. (2001) Calcium-aluminum-rich inclusions in enstatite chondrites (II): oxygen isotopes. *Meteorit. Planet. Sci.* **36**, 223–230.

Fitoussi C. and Bourdon B. (2012) Silicon isotope evidence against an enstatite chondrite earth. *Science* **335**, 1477–1480.

Gooding J. L. and Keil K. (1981) Relative abundances of chondrule primary textural types in ordinary chondrites and their bearing on conditions of chondrule formation. *Meteoritics* **16**, 17–42.

Gray M. L., Weisberg M. K., Ebel D. S., Alexander C. M. O'D., Howard K. T. (2021) Abundances and isotopic compositions of volatiles (H, N, C) in unequilibrated enstatite chondrites and the volatile inventories of the terrestrial planets. Lunar and Planetary Science Conference 52, abstract # 2116.

Grossman L. and Steele I. M. (1976) Amoeboid olivine aggregates in the Allende meteorite. *Geochim. Cosmochim. Acta* **43**, 817–829.

Guan Y., Huss G. R., MacPherson G. J. and Wasserburg G. J. (2000) Calcium-aluminum-rich inclusions from enstatite chondrites: indigenous or foreign? *Science* **25**, 1330–1333.

Hashizume K., Takahata N., Naraoka H. and Sano Y. (2011) Extreme oxygen isotope anomaly with a solar origin detected in meteoritic organics. *Nat. Geosci.* **4**, 165–168.

Hertwig A., Defouilloy C. and Kita N. T. (2018) Formation of chondrules in a moderately high dust enriched disk: evidence from oxygen isotopes of chondrules from the Kaba CV3 chondrite. *Geochim. Cosmochim. Acta* **224**, 116–131.

Hertwig A. T., Kimura M., Ushikubo T., Defouilloy C. and Kita N. T. (2019a) The 26Al- 26Mg systematics of FeO-rich chondrules from Acfer 094: two chondrule generations distinct in age and oxygen isotope ratios. *Geochim. Cosmochim. Acta* **253**, 111–126.

Hertwig A., Kimura M., Defouilloy C. and Kita N. T. (2019b) Oxygen isotope systematics of chondrule olivine, pyroxene, and plagioclase in one of the most pristine CV3Red chondrites (Northwest Africa 8613). *Meteorit. Planet. Sci.* **54**, 2666–2685.

Horstmann M., Humayun M. and Bischoff A. (2014) Clues to the origin of metal in Almahata Sitta EL and EH chondrites and implications for primitive E chondrite thermal histories. *Geochim. Cosmochim. Acta* **140**, 720–744.

Hubbard A. (2016) Ferromagnetism and particle collisions: applications to protoplanetary disks and the meteoritical record. *Astrophys. J.* **826**, 152–162.

Hutchison R., Bridges J. C. and Gilmour J. D. (2005) Chondrules: chemical, petrographic and chronologic clues to their origin by impact. In: Chondrites and the Protoplanetary Disk, ASP Conference Series (A. N. Krot, E. R. D. Scott, & B. Reipurth, eds.). 341.

Jacquet E., Alard O. and Gounelle M. (2015) The formation conditions of enstatite chondrites: Insights from trace element geochemistry of olivine-bearing chondrules in Sahara 97096 (EH3). *Meteorit. Planet. Sci.* **50**, 1624–1642.

Jacquet E. and Marrocchi Y. (2017) Chondrule heritage and thermal histories from trace element and oxygen isotope analyses of chondrules and amoeboid olivine aggregates. *Meteorit. Planet. Sci.* **52**, 2672–2694.

Jacquet E., Piralla M., Kersaho P. and Marrocchi Y. (2021) Origin of isolated olivine grains in carbonaceous chondrites. *Meteorit. Planet. Sci.* **56**, 13–33.

Javoy M. (1995) The intergral enstatite chondrite model of the earth. *Geophys. Res. Lett.* **22**, 2219–2222.

Javoy M., Balan E., Méheut M., Blanchard M. and Lazzeri M. (2012) First-principles investigation of equilibrium isotopic fractionation of O- and Si-isotopes between refractory solids and gases in the solar nebula. *Earth Planet. Sci. Lett.* **319–320**, 118–127.

Javoy M., Kaminski E., Guyot F., Andrault D., Sanloup C., Moreira M., Labrosse S., Jambon A., Agrinier P., Davaille A. and Jaupart C. (2010) The chemical composition of the Earth: enstatite chondrite models. *Earth Planet. Sci. Lett.* **293**, 259–268.

Jones R. H., Leshin L. A., Guan Y. B., Sharp Z. D., Durakiewicz T. and Schilk A. J. (2004) Oxygen isotope heterogeneity in chondrules from the Mokoia CV3 carbonaceous chondrite. *Geochim. Cosmochim. Acta* **68**, 3423–3438.

Kadlag Y., Tatzel M., Frick D. A. and Becker H. (2019) The origin of unequilibrated EH chondrites – Constraints from in situ analysis of Si isotopes, major and trace elements in silicates and metal. *Geochim. Cosmochim. Acta* **267**, 300–321.

Keil K. (1968) Mineralogical and chemical relationships among enstatite chondrites. *J. Geophys. Res.* **73**, 6945–6976.

Kimura M., Hiyagon H., Lin Y. and Weisberg M. K. (2003) FeO-rich silicate components in the Sahara 97159 (EH3) enstatite chondrite: their mineralogy, oxygen isotopic compositions and origin. *Meteorit. Planet. Sci.* **38**, 389–398.

Kimura M., Weisberg M. K., Lin Y., Suzuki A., Ohtani E. and Okazaki R. (2005) Thermal history of enstatite chondrites from silica polymorphs. *Meteorit. Planet. Sci.* **40**, 855–868.

Kita N. T., Nagahara H., Tachibana S., Tomomura S., Spicuzza M. J., Fournelle J. H. and Valley J. W. (2010) High precision SIMS oxygen three isotope study of chondrules in LL3 chondrites: role of ambient gas during chondrule formation. *Geochim. Cosmochim. Acta* **74**, 6610–6635.

Kita N. T., Tenner T. J., Defouilloy C., Nakashima D., Ushikubo T. and Bischoff A. (2015) Oxygen isotope systematics of chondrules in R3 clasts: a genetic link to ordinary chondrites. *Lunar Planet. Sci. Conf.* **46**, 2053.

Krot A. E., Libourel G., Goodrich C. A. and Petaev M. I. (2004a) Silica-rich igneous rims around chondrules in CR carbonaceous chondrites: evidence for condensation origin from fractionated nebular gas. *Meteorit. Planet. Sci.* **39**, 1931–1955.

Krot A. E., Petaev M. I., Russell S. S., Itohc S., Fagan T. J., Yurimoto H., Chizmadia L., Weisberg M. K., Komatsui M., Ulyanovj A. A. and Keil K. (2004b) Amoeboid olivine aggregates and related objects in carbonaceous chondrites: records of nebular and asteroid processes. *Chem. Erde* **64**, 185–239.

Kruijer T. S., Burkhardt C., Budde G. and Kleine T. (2017) Age of Jupiter inferred from the distinct genetics and formation times of meteorites. *Proc. Natl. Acad. Sci.* **114**(26), 6712–6716.

Kunihiro T., Rubin A. E., McKeegan K. D. and Wasson J. T. (2004) Oxygen-isotopic compositions of relict and host grains in chondrules in the Yamato 81020 CO3.0 chondrite. *Geochim. Cosmochim. Acta* **68**, 3599–3606.

Lehner S. W., Buseck P. R. and McDonough W. F. (2010) Origin of kamacite, schreibersite, and perryite in metal-sulfide nodules of the enstatite chondrite Sahara 97072 (EH3). *Meteorit. Planet. Sci.* **45**, 289–303.

Lehner S. W., McDonough W. F. and Nemeth P. (2014) EH3 matrix mineralogy with major and trace element composition compared to chondrules. *Meteorit. Planet. Sci.* **49**, 2219–2240.

Lehner S. W., Petaev M. I., Zolotov M. Y. and Buseck P. R. (2013) Formation of niningerite by silicate sulfidation in EH3 enstatite chondrites. *Geochim. Cosmochim. Acta* **101**, 34–56.

Libourel G., Krot A. N. and Tissandier L. (2006) Role of gas–melt interaction during chondrule formation. *Earth Planet. Sci. Lett.* **251**, 232–240.

Libourel G. and Portail (2018) Chondrules as direct thermochemical sensors of solar protoplanetary disk gas. *Sci. Adv.* **4**(7), eaar3321.

Lin Y., Ouyang Z. and El Goresy A. (2002) A. FeO-rich silicates and Ca, Al-rich inclusions in Qingzhen and Yamato 691 (EH3) meteorites: evidence for migration of mass in the solar nebula. *Chin. Sci. Bull.* **47**, 150–153.

Lin, Y., El Goresy, A., Boyet, M., Feng, L., Zhang, J. & Hao, J. (2011), Earliest Solid Condensates Consisting of the Assemblage Oldhamite, Sinoite, Graphite and Excess 36S in Lawrencite from Almahata Sitta MS-17 EL3 Chondrite Fragment. In 'Workshop on Formation of the First Solids in the Solar System', Vol. 1639 of LPI Contributions, p. 9040.

Lin Y., Kimura M., Hiyagon H. and Monoi A. (2003) Unusually abundant refractory inclusions from Sahara 97159 (EH3): a comparative study with other groups of chondrites. *Geochim. Cosmochim. Acta* **67**, 4935–4948.

Lusby D., Scott E.R.D. and Keil K. (1987) Ubiquitous high FeO silicates in enstatite chondrites. Proceeding Lunar and Planetary Science Conference 17, Journal of Geophysicl Research. Supplement 92, E679–E695.

Marrocchi Y. and Chaussidon M. (2015) A systematic for oxygen isotopic variation in meteoritic chondrules. *Earth Planet. Sci. Lett.* **430**, 308–315.

Marrocchi Y., Euverte R., Villeneuve J., Batanova V., Welsch B., Ferrière L. and Jacquet E. (2019) Formation of CV chondrules by recycling of amoeboid olivine aggregate-like precursors. *Geochim. Cosmochim. Acta* **247**, 121–141.

Marrocchi Y. and Libourel G. (2013) Sulfur and sulfides in chondrules. *Geochim. Cosmochim. Acta* **119**(2013), 117–136.

Marrocchi Y., Villeneuve J., Batanova V., Piani L. and Jacquet E. (2018) Oxygen isotopic diversity of chondrule precursors and the nebular origin of chondrules. *Earth Planet. Sci. Lett.* **496**, 132–141.

Nagahara H., Kita N. T., Ozawa K. and Morishita Y. (2008) Condensation of major elements during chondrule formation and its implication to the origin of chondrules. *Geochim. Cosmochim. Acta* **72**, 1442–1465.

Nittler L. R., Starr R. D., Weider S. Z., McCoy T. J., Boynton W, V., Ebel D. S., Ernst C. M., Evans L. G., Goldsten J. O., Hamara D. K., Lawrence D. J., McNutt R. L. Jr., Schlemm C. E. II, Solomon S. C. and Sprague A. L. (2011) The major-element composition of Mercury's surface from MESSENGER X-ray spectrometry. Science 333, 1847–1850.

Paniello R., Day J. M. D. and Moynier F. (2012) Zn isotopic evidence for the origin of the Moon. *Nature* **490**, 376–379.

Piani L., Marrocchi Y., Libourel G. and Tissandier L. (2016) Magmatic sulfides in the porphyritic chondrules of EH enstatite chondrites. *Geochim. Cosmochim. Acta* **195**, 84–99.

Piani L., Marrocchi Y., Rigaudier T., Vacher L. G., Thomassin D. and Marty B. (2020) Earth's water may have been inherited from material similar to enstatite chondrite meteorites. *Science* **369**, 1110–1113.

Pouchou J. L. and Pichoir F. (1991) Quantitative analysis of homogeneous or stratified microvolumes applying the model "PAP". In *Electron Probe Quantitation* (eds. K. F. J. Heinrich and D. E. Newbury). Plenum Press, New York, NY, pp. 31–75.

Rambaldi E. R., Rajan R. S., Wang D. and Housley R. M. (1983) Evidence for RELICT grains in chondrules of Qingzhen, an E3 type enstatite chondrite. *Earth Planet. Sci. Lett.* **66**, 11–24.

Rubin A. E. (1983) The Adhi Kot breccia and implications for the origin of chondrules and silica-rich clasts in enstatite chondrites. *Earth Planet. Sci. Lett.* **64**, 201–212.

Rudraswami N. G., Ushikubo T., Nakashima D. and Kita N. T. (2011) Oxygen isotope systematics of chondrules in Allende CV3 chondrite: high precision ion microprobe studies. *Geochim. Cosmochim. Acta* **75**, 7596–7611.

Sakamoto N., Seto Y., Itoh S., Kuramoto K., Fujino K., Nagashima K., Krot A. N. and Yurimoto H. (2007) Remnants of the early solar system water enriched in heavy oxygen isotopes. *Science* **317**, 231–233.

Savage P. S. and Moynier F. (2013) Silicon isotopic variation in enstatite meteorites: clues to their origin and Earth-forming material. *Earth Planet. Sci. Lett.* **361**, 487–496.

Schneider J. M., Burkhardt C., Marrocchi Y., Brennecka G. A. and Kleine T. (2020) Early evolution of the solar accretion disk inferred from Cr-Ti-O isotopes in individual chondrules. *Earth Planet. Sci. Lett.* **551** 116585.

Schrader D. L., Connolly, Jr., H. C., Lauretta D. S., Nagashima K., Huss G. R., Davidson J. and Domanik K. J. (2013) The formation and alteration of the Renazzo-like carbonaceous chondrites II: linking O-isotope composition and oxidation state of chondrule olivine. *Geochim. Cosmochim. Acta* **101**, 302–327.

Schrader D. L., Nagashima K., Davidson J., McCoy T. J., Ogliore R. C. and Fu R. R. (2020) Outward migration of chondrule fragments in the early Solar System: O-isotopic evidence for rocky material crossing the Jupiter Gap? *Geochim. Cosmochim. Acta* **282**, 133–155.

Schrader D. L., Nagashima K., Krot A. N., Ogliore R. C. and Hellebrand E. (2014) Variations in the O-isotope composition of gas during the formation of chondrules from the CR chondrites. *Geochim. Cosmochim. Acta* **132**, 50–74.

Schrader D. L., Nagashima K., Krot A. N., Ogliore R. C., Yin Q.-Z., Amelin Y., Stirling C. H. and Kaltenbach A. (2017) Distribution of ^{26}Al in the CR chondrite chondrule-forming region of the protoplanetary disk. *Geochim. Cosmochim. Acta* **201**, 275–302.

Sikdar J. and Rai V. K. (2020) Si-Mg isotopes in enstatite chondrites and accretion of reduced planetary bodies. *Sci. Rep.* **10**, 1273.

Simon S. B., Sutton S. R. and Grossman L. (2016) The valence and coordination of titanium in ordinary and enstatite chondrites. *Geochim. Cosmochim. Acta* **189**, 377–390.

Tanaka R. and Nakamura E. (2017) Silicate-SiO reaction in a protoplanetary disk recorded by oxygen isotopes in chondrules. *Nat. Astron* **1**, 0137.

Tenner T. J., Ushikubo T., Kurahashi E., Kita N. T. and Nagahara H. (2013) Oxygen isotope systematics of chondrule phenocrysts from the CO3.0 chondrite Yamato 81020: Evidence for two distinct oxygen isotope reservoirs. *Geochim. Cosmochim. Acta* **102**, 226–245.

Tenner T. J., Nakashima D., Ushikubo T., Kita N. T. and Weisberg M. K. (2015) Oxygen isotope ratios of FeO-poor chondrules in CR3 chondrites: influence of dust enrichment and H_2O during chondrule formation. *Geochim. Cosmochim. Acta* **148**, 228–250.

Tenner T. J., Kimura M. and Kita N. T. (2017) Oxygen isotope characteristics of chondrules from the Yamato-82094

ungrouped carbonaceous chondrite: further evidence for common O-isotope environments sampled among carbonaceous chondrites. *Meteorit. Planet. Sci.* **52**, 268–294.

Tissandier L., Libourel G. and Robert F. (2002) Gas-melt interactions and their bearing on chondrule formation. *Meteorit. Planet. Sci.* **37**, 1377–1389.

Trinquier A., Elliott T., Ulfbeck D., Coath C., Krot A. N. and Bizzarro M. (2009) Origin of nucleosynthetic isotope heterogeneity in the Solar protoplanetary disk. *Science* **324**, 374–376.

Ushikubo T., Kimura M., Kita N. T. and Valley J. W. (2012) Primordial oxygen isotope reservoirs of the solar nebula recorded in chondrules. *Geochim. Cosmochim. Acta* **90**, 242–264.

Van Niekerk D. and Keil K. (2011) Metal/sulfide silicate intergrowth textures in EL3 mreteorites: origin by impact melting on the EL parent body. *Meteorit. Planet. Sci.* **46**, 1484–1497.

Warren P. H. (2011) Stable-isotopic anomalies and the accretionary assemblage of the Earth and Mars: a subordinate role for carbonaceous chondrites. *Earth Planet. Sci. Lett.* **311**, 93–100.

Weisberg M. K., Ebel D. S. and Connolly H. C. Jr. (2013) EL3 chondrites: primitive nebular materials, not products of asteroidal Processing. 44th Lunar and Planetary Science Conference, abstract # 2871.

Weisberg M. K., Ebel D. S., Connolly, Jr., H. C., Kita N. T. and Ushikubo T. (2011) Petrology and oxygen isotope compositions of chondrules in E3 chondrites. *Geochim. Cosmochim. Acta* **75**, 6556–6569.

Weisberg M. K. and Kimura M. (2012) The unequilibrated enstatite chondrites. *Chem. Erde* **72**, 101–115.

Weisberg M. K., Prinz M. and Fogel R. A. (1994) The evolution of enstatite and chondrules in unequilibrated enstatite chondrites: evidence from iron-rich pyroxene. *Meteoritics* **29**, 362–373.

Weisberg M. K., Ebel D. S., Kimura M., Kita N. T., and Nakashima D. (2010) Petrology and oxygen isotopes of chondrules in the Kota-Kota EH3 Chondrite. 41st Lunar and Planetary Science Conference, abstract #1756.

Weyrauch M., Horstmann M. and Bischoff A. (2018) Chemical variations of sulfides and metal in enstatite chondrites—Introduction of a new classification scheme. *Meteorit. Planet. Sci.* **53**, 394–415.

Williams C. D., Sanborn M. E., Defouilloy C., Yin Q.-Z., Kita N. T., Ebel D. S., Yamakawa A. and Yamashita K. (2020) Chondrules reveal large-scale outward transport of inner Solar System materials in the protoplanetary disk. *Proc. Natl. Acad. Sci.* **117**, 23426–23435.

Young E. D. and Russell S. S. (1998) Oxygen reservoirs in the early solar nebula inferred from an Allende CAI. *Science* **282**, 452–455.

Yu Y., Hewins R. H., Clayton R. N. and Mayeda T. K. (1995) Experimental-study of high temperature oxygen-isotope exchange during chondrule formation. *Geochim. Cosmochim. Acta* **59**, 2095–2104.

Yurimoto H. and Wasson J. T. (2002) Extremely rapid cooling of a carbonaceous-chondrite chondrule containing very ^{16}O-rich olivine and a ^{26}Mg-excess. *Geochim. Cosmochim. Acta* **66**, 4355–4363.